Spring 2021

Mechanical activation and cation site disorder of spinel-based ceramics

Cole A. Corlett

Department:

MECHANICAL ACTIVATION AND CATION SITE DISORDER OF SPINEL-BASED CERAMICS

by

COLE ALEXANDER CORLETT

A THESIS

Presented to the Graduate Faculty of the

MISSOURI UNIVERSITY OF SCIENCE AND TECHNOLOGY

In Partial Fulfillment of the Requirements for the Degree

MASTER OF SCIENCE IN MATERIALS SCIENCE AND ENGINEERING

2021

Approved by:

William G. Fahrenholtz, Advisor
Jeremy L. Watts
Wayne Huebner

PUBLICATION DISSERTATION OPTION

This thesis consists of the following two articles, formatted in the style used by the Missouri University of Science and Technology:

Paper I: Pages 14-29 will be submitted as a paper to the Journal of the European Ceramic Society.

Paper II: Pages 30-47 will be submitted as a paper to the Journal of Ceramics International.

ABSTRACT

This research focuses on the processing and the effects that has on the cation disorder of magnesium-aluminate spinel based ($MgAl_2O_4$) ceramics. The first goal of this project was to determine the effects of high-energy milling, i.e., mechanical activation, on cation disorder (inversion) within the spinel structure. First, 1:1 molar ratios of MgO:Al_2O_3 ceramics were processed using two green processing methods, ball milling (XD) and SPEX milling (mechanical activation, MA) followed by a subsequent annealing treatment in air to form a single spinel phase in each powder sample. Neutron diffraction analysis was employed to determine the cation site occupancy and revealed that overall mechanical activation resulted in a lower degree of cation site inversion compared to the non-activated materials, about 0.12 was the largest value returned for the MA materials and 0.13 was the lowest value out of the XD samples. The second portion of this project was to investigate the synthesis, densification behavior, and crystallographic site occupancy for a high-entropy spinel (HES) $(Co_{0.2}Cu_{0.2}Mg_{0.2}Ni_{0.2}Zn_{0.2})Al_2O_4$. This was compared to several other compositions including a $MgAl_2O_4$, $NiAl_2O_4$ and $(Mg_{0.5}Ni_{0.5})Al_2O_4$ (MAS, NAS, NMAS) specimens produced using the same methods. Each composition reacted to form a single phase, but analysis of x-ray diffraction (XRD) patterns revealed that the HES specimen had a degree of inversion of 0.4. The NAS and NMAS samples were also highly inverted whereas the MAS material had minimal cation disorder.

ACKNOWLEDGEMENTS

First, I would like to thank my advisor, Dr. Bill Fahrenholtz, for his guidance and patience over the last two years. His council was enlightening for myself, as someone from outside the materials and ceramics field. I thank him for allowing me the opportunity to travel the country to see current research being performed. Most of all, I would like to thank him for the advice he gave to me in regard to choices that would be best for my family. Next, I would like to thank Dr. Jeremy Watts for his invaluable assistance in the laboratory. Without his guidance in machine/instrument trouble shooting, I would have never made it through the past two years.

Thank you to my peers in 307 for all of your help and support. They taught me how to operate (and sometimes repair) much of the equipment necessary for my research. They kept me accountable when I needed it most, provided sound advice and increased my understanding of materials processing and characterization. Not only did they do that, but they are also enjoyable to with, even during the "pushes" for results when things were busiest. Thank you also to all the undergraduate research who contributed to this body of research, your help and input was invaluable.

Most importantly, I would not be here with the love and support of my family. To my mothers and fathers, I won't fully understand the sacrifices the four of you have made as I have grown, until I make those same sacrifices for my own kids. I truly appreciate everything. To my wife, Marissa Corlett, you have supported me every step of the way and encouraged me to stick with this journey of mine.

TABLE OF CONTENTS

Page

PUBLICATION THESIS OPTION iii

ABSTRACT iv

ACKNOWLEDGEMENTS v

LIST OF ILLUSTRATIONS viii

LIST OF TABLES ix

SECTION

1. INTRODUCTION 1

2. LITERATURE REVIEW 3

2.1 SPINEL 3

2.1.1 Crystallography 4

2.1.2 $MgAl_2O_4$ Spinel Formation 7

2.2 MECHANICAL ACTIVATION 9

2.3 HIGH ENTROPY MATERIALS 11

PAPER

I. MECHANICAL ACTIVATION AND CATION SITE DISORDER IN $MgAl_2O_4$ 14

ABSTRACT 14

1. INTRODUCTION 15

2. EXPERIMENTAL PROCEDURE 16

2.1 PROCESSING 16

2.2 CHARACTERIZATION 17

3. RESULTS & DISCUSSION 19

4. SUMMARY 26

ACKNOWLEDGEMENTS 26

REFERENCES 27

II. SYNTHESIS AND CHARACTERIZATION OF A HIGH ENTROPY SPINEL 30

ABSTRACT 30

1. INTRODUCTION 30

2. EXPERIMENTAL PROCEDURE 31

3. RESULTS & DISCUSSION 34

4. SUMMARY 44

ACKNOWLEDGEMENTS 44

REFERENCES 45

SECTION

3. CONCLUSIONS 48

4. FUTURE WORK 50

REFERENCES 52

VITA 59

LIST OF ILLUSTRATIONS

Figure Page

SECTION

2.1. Ideal, normal spinel unit cell where the red spheres are oxygen anions and the blue and green are magnesium and aluminum cations, respectively. 5

2.3. The structural diversity of high entropy ceramics with the central image showing a supercell of rock-salt structure with dark grey anions and random cations of different colors. 13

PAPER I

1. XRD patterns of the heat-treated MA (A) and XD (B) powders. 20

2. Representative neutron diffraction pattern for XD1500C with the Rietveld refinement fit. 21

3. Inversion parameter vs. calcination temperature plotted for the spinel powders. 25

PAPER II

1. XRD patterns of reacted spinel powders. 35

2. SEM micrographs of a) as-mixed b) milled HES powders after annealing at 1200 °C for 2 hours. The red circle highlights a larger particle present in the mixed material that is largely missing from the milled powder. 40

3. Relative density as a function of sintering time for HES powders. The sintering time begins when pressure was applied to the powder compacts. The vertical lines denote when the compacts reached the final sintering temperature. 41

4. a) Representative Vickers indent of the hot pressed HES material sintered at 1375 °C b) representative image of grain size boundaries in HES material. 43

LIST OF TABLES

Table Page

PAPER I

1. Peak listing of sample XD1500C displayed in Figure 2. 21

2. The table shows the site occupation in percent. Al2 and Mg1 are on 16c, Mg2 and Al1 are on 8b. Standard crystallographic cell Wyckoff sequence ecb. 23

PAPER II

1. Indexed peaks of the four spinel materials. 37

2. Summary of Rietveld refinement of the spinel powders. 38

3. Specific surface area and theoretical particle size of unreacted prepared powders. 41

4. Densification rates and final densities for the three hot-pressed HES specimens. 42

5. Vickers hardness values and grain sizes for hot pressed HES samples. 43

1. INTRODUCTION

The research in this thesis examines the atomic and microstructural properties of ceramics with the spinel crystal structure. Spinel ceramics have various industrial applications in catalyst-supports, refractories, transparent and radiation-tolerant ceramics.[1-3] Mechanical activation of spinel-based ceramics has the potential to alter the spinel formation temperature and the degree of site inversion in the crystal structure, thus, reducing energy costs during production and leading to lower overall production cost. The research being conducted will be of interest for armor, optical, nuclear, and various other applications.

Magnesium aluminate ($MgAl_2O_4$) is the solitary compound in the MgO-Al_2O_3 binary system. It has the spinel structure and is utilized due to its high melting point, excellent mechanical properties, corrosion resistance and its ability to become optically transparent.[4,5] More generally, ceramics with the spinel structure have been investigated because of their extensive use in industrial applications. Raw materials for spinel ceramics are easily found in the earth's crust. Previous studies have shown that the occupancy of lattice sites of $MgAl_2O_4$ can be altered by changing the sintering temperature and duration.[6] In naturally occurring magnesium aluminate, Mg atoms occupy tetrahedral sites in the lattice while Al atoms occupy octahedral sites. However, synthetic spinel ceramics exhibit disorder in site occupancy that can reach as high as 30%.[7,8]

Various methods can be employed to alter the degree of disorder in site occupancy in $MgAl_2O_4$. The method used in this research study is the one of mechanical activation (MA) – a high energy milling process that induces physical and chemical

changes in materials that increases the chemical activity and potential energy of the activated material. This change in energy comes from altering the specific surface area and raising the internal energy and generally increasing the free energy of the system. During MA, the crystallite size is reduced by impact and attrition, which may lead to alterations or defects within the crystal structure.[9] The mechanical forces involved lead to elastic and plastic deformation, which changes the physiochemical properties of the material.[10] The reactivity of solid materials is increased by structural changes due to generation of point defects, line defects, volume defects, and electronic defects. These various changes suggest that the mechanical energy of the process is transformed into crystal lattice defects, leading to fragmentation, particle size reduction and changes in the specific surface area and the physiochemical properties of the crushed material. MA is commonly used as a pre-sintering technique to improve the reactivity and sinterability of materials.[11,12]

The effect of composition and temperature on cation disorder within the spinel structure was studied extensively to determine the viability of mechanical activation as an approach to altering the degree of inversion. Paper 1 of this thesis focuses on the effect mechanical activation has on the inversion parameter of synthesized $MgAl_2O_4$ and will be submitted to the *Journal of the European Ceramic Society* for publication. Additionally, studying a high entropy material within the spinel system will allow for a more comprehensive understanding of materials processing. The second paper of this thesis focuses on the synthesis and characterization of the $(Mg_{0.2},Cu_{0.2},Co_{0.2},Ni_{0.2},Zn_{0.2})Al_2O_4$ high entropy spinel material and will be submitted to the *Journal of Ceramics International* for publication.

2. LITERATURE REVIEW

The magnesia-alumina (MgO-Al_2O_3) binary phase system includes materials used in industrial applications including armor, refractories, catalyst-supports, and radiation-tolerant ceramics.[1-7] The one stable compound in the system, magnesium aluminate, also referred to informally as spinel, ($MgAl_2O_4$), is the mineral name for the compounds that serves as the prototype for the class of compounds labeled as "spinels." The spinel class of materials covers a wide range of chemistries and they each have varying tendencies for site occupancy disorder. This class of materials is ideal for studying how various process parameters affects the disorder of the cation site occupancy within the structure.

2.1. SPINEL

The term spinel is often confusing because it refers to a material that has the spinel structure (AB_2X_4 or $B(AB)X_4$) and the compound magnesium aluminate, "spinel," ($MgAl_2O_4$). In general, spinel is typically written in the form AB_2X_4, where A represents the cation that fills 1/8 of the tetrahedral sites and B represents the cation that fills 1/2 the octahedral sites, and X is an anion in a close packed arrangement. Spinel occurs naturally as a gemstone with a Mohs hardness of 7.5 – 8.0. Hundreds of materials have been discovered with various chemistries that crystallize in the spinel structure. It would be difficult to compile a list of all these chemistry variants, but many of these various spinels have been studied extensively. There are many options for the anion, X, to be: O, Si, Se, Te, S or N.

2.1.1. Crystallography. Magnesium aluminate spinel is the parent compound of the spinel family and was first studied independently by Bragg[13] and Nishikawa.[14] The structure, as seen in Figure 2.1, was first reported with all the Mg^{2+} cations on tetrahedral sites and all of the Al^{3+} cations on octahedral sites within a face centered cubic (FCC) Bravais lattice. Spinel demonstrates the $\boldsymbol{F\bar{4}3m}$ space group,[15] but the simpler $\boldsymbol{Fd3m}$, is generally used.[16] The oxygen ions take the form of a cubic-closed packed (ccp) spatial arrangement. The $MgAl_2O_4$ unit cell consists of eight formula units: 56 total atoms – 32 oxygen anions and 24 cations. The spinel lattice parameter, 8.083 Å, is larger than many oxides, but the unit cell volume is eight times that of the ccp oxygen sublattice unit cell. Of the 64 tetrahedral sites, eight are occupied by Mg^{2+} cations and of the 32 octahedral sites half are occupied by Al^{3+} cations. The structure can also be described using Wyckoff notation for a more formal approach. Within the *Fd3m* space group, the Mg^{2+} cations occupy 8a and Al^{3+} cations occupy 16*d* Wyckoff positions. The O^{2-} anions occupy 48*f* Wyckoff positions. The oxygen positional parameter, (u), measure how far the oxygen positions are displaced in the <111> directions from the ideal FCC positions. This parameter is typically equivalent to about 0.1 Å, which corresponds with a shift away from the divalent Mg^{2+} (tetrahedral site expansion while octahedral site volume decreases).[18] As seen in this current study, the spinel compound is ideally composed of equimolar MgO and Al_2O_3.

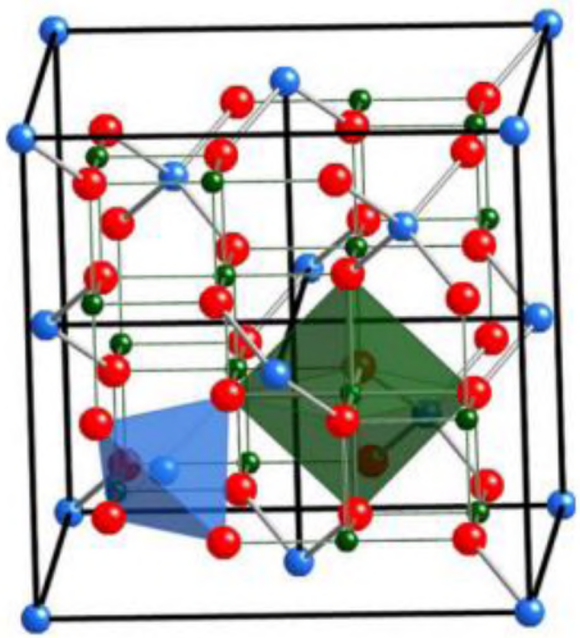

Figure 2.1. Ideal, normal spinel unit cell where the red spheres are oxygen anions and the blue and green are magnesium and aluminum cations, respectively.[17]

In 1931, Barth and Posnjak[18-20] discovered that two structural spinel arrangements exist. 'Normal' (AB_2X_4) spinel, the one previously discovered by Bragg and Nishikawa, and one with 'variate atom equipoints' ($ABAX_4$), which was later designated as 'inverse' spinel by Verwey and Heilmann.[21] A structure with 'variate atom equipoints' or cation disorder, the A cation fills 8 tetrahedral sites as well as 8 of the octahedral sites, while the B cation fills the other 8 octahedral sites.

Verwey and Heilmann[21] further defined spinel as either 'normal' 2-3 spinel or 'inverse' 3-2 spinel, where the 2 and 3 refer to divalent and trivalent cations. Cation disorder falls between these two extremes, giving rise to partially inverse spinels. The general formula for the unit cell of a 2-3 spinel is given by:

$$(X^{2+}_{1-i}Y^{3+}_{i})^{A_{IV}}_{8}[X^{2+}_{\frac{i}{2}}Y^{3+}_{\frac{2-i}{2}}]^{B_{VI}}_{16}O_{32}\begin{cases} i = 0 \rightarrow normal\ spinel \\ i = 2/3 \rightarrow random\ cation\ arrangement \\ i = 1 \rightarrow inverse\ spinel \end{cases} \quad (1)$$

Where X^{2+} and Y^{3+} are divalent and trivalent cations.[22] The fraction of tetrahedral-sites occupied by trivalent ions is referred to as i, or the inversion parameter. There is also an 'inverse' 4-2 spinel that is composed of quadrivalent and divalent cations, where the tetrahedral-sites are filled by divalent cations and the octahedral-sites are occupied by both divalent and quadrivalent cations in equal proportions.

Sickafus[16,22] completed a rather extensive review of previous research on $MgAl_2O_4$ spinel. Various authors state that the degree of inversion for $MgAl_2O_4$ spinel can be measured by using several techniques, including but not limited to neutron diffraction (ND) infrared (IR) absorption and nuclear magnetic resonance (NMR). Other methods include electrical conductivity, x-ray diffractometry (XRD), and Mössbauer spectroscopy have been used to determine the inversion factor in other spinel compounds.

The final chemistry for spinel compounds is controlled by at least 3 variables. These variables are the oxygen positional parameter, *u*, the lattice parameter, a, and the cation inversion parameter, *i*. The *u* parameter changes with the radius (of the cations), r(Å), meaning that the A and B-site volumes are adjusted to best fit the cations, thus the bond lengths adjust by variations in u. The lattice parameter, *a*, varies with the average of the A and B site cationic radii. Several things influence inversion - temperature, the electrostatic contribution to the lattice energy, cationic radii, cationic charge, and crystal-field effects. Wood[23] previously studied the degree of inversion in $MgAl_2O_4$ in 1986. They determined the rate of cation redistribution is very slow below 725 °C but above 925 °C the redistribution occurs so rapidly that all samples heat treated and quenched

above 925 °C have about the same equilibrium distribution as that of samples heat treated at 925 °C after quenching. The cation disorder or inversion, in $MgAl_2O_4$ can be described by the reaction:

$$Mg_{Mg}^{x} + Al_{Al}^{x} \leftrightarrow Al_{Mg}^{\cdot} + Mg_{Al}^{\prime} \qquad (2)$$

The normal 2-3 spinel will satisfy the Verwey-Heilmann principle of maximal charge neutralization,[21] but in the case of the inverse 2-3 spinel, it is not fulfilled. This is from the cation radii and charge effects counteracting each other. The above principle above states, "if neutralization of charge is to be sharply localized around cations, then cations of high valence will have large coordination numbers, so as to be neutralized efficiently by numerous anions in the first coordination shell." The problem that arises with this is that high-valence cations generally have small ionic radii, which, according to Pauling's first rule, the cations may be undersized enough to have movement between the anions. Pauling's first rule states, "as cation valence increases, small interstices and small coordination numbers become preferable" and is quantified by the maximum radius ratio, R_A/R_X, where A is a cation and X is an anion, below this value the cation would be unstable in its site. Inversion in spinels is partially due these two ideas competing with one other.

2.1.2. $MgAl_2O_4$ Spinel Formation. In its naturally occurring mineral, $MgAl_2O_4$ spinel forms as highly ordered (i=0) due to the slow crystallization over geological times. Magnesium aluminate made synthetically has some appreciable amount of disorder and can formed rich in either MgO or Al_2O_3.[24,25] When stoichiometric spinel is formed from the parent magnesia and alumina oxides, there is a 5 – 8% volume expansion.[26] Many attempts have been made experimentally to form pure, stoichiometric

spinel. The formation of spinel has been studied numerous times as a solid-state reaction, co-precipitation, hydrothermal technique, spray pyrolysis, sol-gel, magnesium aluminum double alkoxide, controlled hydrolysis of metal alkoxides decomposition of organometallic compounds in supercritical fluids and an aerosol method.[27-32] Generally a two-stage sintering process is often used as it aids in densification. The process typically includes an initial hold temperature between 900 and 1200 °C (used for spinel formation) and the second stage used for densification is in the range of 1600 – 1800 °C.[33]

Bratton[28,34] first investigated a co-precipitation method for forming stoichiometric $MgAl_2O_4$ using hydroxides and determined that maximum densification could be achieved when the co-precipitate was calcined at 860 °C; above this temperature the final sintered density decreased. Using the aforementioned procedure, Bratton studied hot-pressing phenomena of spinel in 1972 using pre-reacted spinel powder.[35] This study proved to be successful in that many high density (<95% theoretical) were produced at temperatures as low as 1400 °C with an applied pressure of ~35MPa.

Hot pressing is one of several pressure-assisted sintering techniques in which an external pressure is applied to the powder compact during a large portion of the heating schedule. This enhances the driving force for densification while also limiting grain growth. This added pressure can also lead to faster densification, lower sintering temperatures and a shorter sintering time. In general practice, pressure assisted sintering can nearly always guarantee the production of ceramics with high density and fine grain size.[36] Since then, numerous studies have been completed using various forms of pressure assisted sintering, with more recent attempts focusing on producing transparent magnesium aluminate.[37-39]

Pressure assisted sintering has proven to be a successful method for producing dense ceramics.[36] This technique and others involving mechanical activation (to be discussed in the next section) has been adopted for all spinel compounds produced during experimentation.

2.2. MECHANICAL ACTIVATION

The traditional method for synthesizing magnesium aluminate spinel involves a solid-state reaction between oxides (or hydroxides or salts) of aluminum and magnesium. This straightforward approach has a couple disadvantages, namely low surface area and chemical inhomogeneity. These shortcomings can be overcome by additional processing steps to reduce particle size and create a more uniform material composition.

Mechanical activation is an efficient method when particle size reduction, mixing, and lowering the required thermal treatment temperatures are all necessary goals. Synthesis of spinel by a mechanochemical activation process was previously studied by Mackenzie et al. in 2000.[40] This study proved to be successful in that they managed to synthesize pure magnesium aluminate, but likely due to the crystallite size of the precursor materials of $Al_2(OH)_3$ and $MgCO_3$, the reaction temperatures were in the range of 1400 – 1600 °C.

With comminution, the interest is mainly in achieving certain physical characteristics, such as particle size and distribution. Grinding increases the chemical reactivity of powders. Rupture of the bonds during particle fracture creates surfaces with unfilled valences – this combined with a high surface area leads to a reaction between mixed particles or the particles and their surroundings.[41]

Preparing powders by high energy ball milling of elemental mixtures is known by various terms, including mechanochemical synthesis, high energy milling, mechanical activation, and several other terms. While no one term appears to have become standard, mechanical activation will be used for the remainder of this thesis to describe high energy milling.

Mechanical activation can be performed in small mills, such as the Spex mill for synthesizing of a few grams of powder. Larger quantities may be milled in attrition or planetary ball mills if needed. When using a Spex mill, a cylindrical vial containing the milling balls (5-10 mm in diameter) and the powder charge is treated to large amplitude vibrations in three dimensions at a frequency of approximately 20 Hz. The powder material generally takes up roughly 20% of the volume of the vial with the milling media accounting for another 40 – 60% (about 3 times the volume of the powder). Milling in this manner can be done for very extended time periods (tens of hours) or also quite short time periods as particle size reduction happens much more readily than with a lower energy ball milling technique.

Tavangarian[42] investigated the synthesis of $MgAl_2O_4$ after mechanical activation of Al_2O_3 and $MgCO_3$ with post annealing at 1200 °C. This study proved successful in that pure nanocrystalline spinel was fabricated after 5 hours of mechanical activation with a post thermal treatment at 1200 °C. This material had a crystallite size of about 45 nm and further milling appeared to have no further effect on the structure or composition of the spinel phase after calcination.

Numerous studies examined composition and temperature effects on cation disorder within the spinel structure,[43-48] but to the author's best knowledge, the amount of

information related to mechanical activation and its effects on cation disorder in $MgAl_2O_4$ is limited to the study by Obradovic[50] that led to this present investigation. In the study, the cation site occupancy in $MgAl_2O_4$ was investigated using various methods. It was determined that mechanical activation lowered the spinel formation temperature by approximately 200 °C and the corresponding activation energy by about 25%. Raman spectroscopy was used to characterize the degree of inversion as a function of sintering temperature. The Raman spectra collected indicated that beyond 1400 and 1500 °C for the activated and non-activated samples, respectively, the crystal structure had reordered itself.

2.3. HIGH ENTROPY MATERIALS

In the last several years, the idea of high entropy has been explored in various classes of materials, ranging from high entropy alloys (HEAs)[51] to high entropy carbides (HECs),[52] borides (HEBs)[53], and to high entropy oxides (HEOs)[54]. The concept of HEAs and multiprincipal component alloys was initially proposed independently in 2004 by Yeh and co-workers[55] and Cantor *et al*[56]. The largest driving force for this research was to explore the unexplored regions of the multicomponent phase diagrams – entropy was left unmentioned by Cantor. Yeh, however, looked to maximize the configuration entropy to avoid intermetallic phases and instead focused on stabilizing solid solution phases. This ultimately led to the nomenclature used today to describe high entropy materials (HEMs) such as HEA, HEB, HEC, and HEO. Rost[57] first showed entropic stabilization of five different cations in equimolar ratios into a single-phase oxide system. This opened the door to entropy stabilized materials beyond metals.

The existence of HEOs is surprising since enthalpy-dominated phase separation is common in oxide phase diagrams.[57] HEOs are characterized by the random arrangement of cations on their sublattice while the oxygen ions remain in their sub-lattice.[58] One of the first HEOs studied was $(Co_{0.2},Cu_{0.2},Mg_{0.2},Ni_{0.2},Zn_{0.2})O$ with a rock salt structure with only one Wyckoff position for the cation. Shortly after this, fluorite, perovskite, and spinel-based HEOs were synthesized. It should be noted that spinel and perovskite structures both have more than one Wyckoff position, but the rock salt and fluorite structures only have one.[59] Even so, the corresponding HEOs can be synthesized by replacing one or both Wyckoff sites of the cation. Figure 2.3 displays the structural diversity available with various high entropy ceramics[60]. The unique chemistry of HEOs (and all HEMs) leads to a multifunctional behavior that includes a combination of dielectric, magnetic, thermal, and catalytic properties in a single HEO such as (Co,Cu,Mg,Ni,Zn)O.

In 2017, Dabrowa,[61] was the first to synthesize a HEO, $(Co,Cr,Fe,Mn,Ni)_3O_4$, with the spinel structure (*Fd3m* space group). The intent of that study was to confirm that these cations behaved the same in oxide systems as they do in high entropy alloy systems, given that the cations have similar atomic radii and have good solubility in binary and ternary systems. That study appears successful in that x-ray diffraction (XRD) results indicated a pure, single-phase spinel material was synthesized from the constituent parent oxides. This was further confirmed via energy dispersive spectroscopy (EDS) mapping of the sample. Grzesik in 2020, investigated the defect structure and transport properties of the same $(Co,Cr,Fe,Mn,Ni)_3O_4$ spinel. They were able to determine, based on thermogravimetric studies, that a defect inversion phenomenon occurs at high oxygen

partial pressures, the dominating type of defect appeared to change from oxygen vacancies to interstitial oxygen.[6]

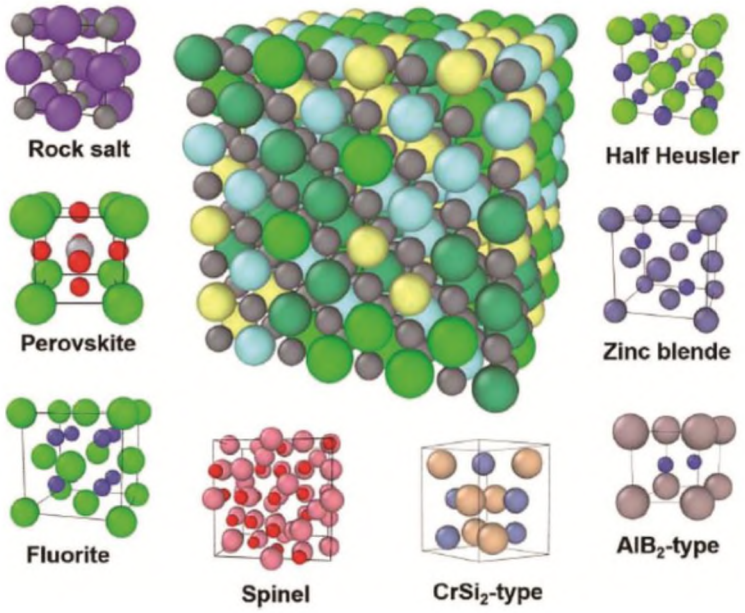

Figure 2.3. The structural diversity of high entropy ceramics with the central image showing a supercell of rock-salt structure with dark grey anions and random cations of different colors.[60]

PAPER

I. MECHANICAL ACTIVATION AND CATION SITE DISORDER IN $MgAl_2O_4$

Cole A. Corlett[1], Matthias D. Frontzek[2], N. Obradovic[3], Jeremy L. Watts[1], William G. Fahrenholtz[1]

[1]Missouri University of Science & Technology, Rolla, MO, USA

[2]Neutron Scattering Division, Oak Ridge National Laboratory, Oak Ridge, TN, USA

[3] Institute of Technical Sciences of SASA, Knez Mihailova 35/IV, 11000 Belgrade, Serbia

ABSTRACT

The synthesis and crystallographic site occupancy were investigated for $MgAl_2O_4$ with and without mechanical activation of the precursor powders. Heating to 1200°C or higher resulted in the formation of a single spinel phase regardless of whether the powders were mechanically activated or not. Neutron diffraction analysis was used to determine cation site occupancy and revealed that mechanical activation resulted in a lower degree of cation site inversion compared to the non-activated materials. This was the first study to characterize the effects of mechanical activation on crystallographic site occupancy in magnesium aluminate spinel using neutron diffraction.

Keywords: spinel, neutron diffraction, inversion, mechanical activation

1. INTRODUCTION

Magnesium aluminate spinel, $MgAl_2O_4$, is the only compound in the MgO-Al_2O_3 binary system. It is the prototype for the spinel structure and is attractive due to its high melting point, corrosion resistance, mechanical properties, and low cost.[1,2] Many different routes have been used to synthesize spinel-based ceramics, including direct solid-state reactions of oxides, wet chemical precipitation, and mechanical activation (MA).[3-6,8-11] For most applications, the choice of synthesis method is based on the desired particle size and purity of the spinel powder.

In naturally occurring $MgAl_2O_4$ spinel, Mg atoms (designated A cation herein) occupy one-eighth of the tetrahedral sites in the lattice.[12] Similarly, Al atoms (designated B cation herein) occupy one-half of the octahedral sites. Due to similar cation radii, Mg can occupy some octahedral sites and Al atoms can occupy some tetrahedral sites, a process that is called inversion. The partially inverted structure can be represented as $(A_{1-i}B_i)$-$[A_iB_{2-i}]Z_4$, where i is the inversion parameter, with tetrahedral site occupancy given in parentheses () and octahedral site occupancy given in square brackets [].[13] Site inversion in synthetic $MgAl_2O_4$ can range from 0.1 to 0.6, but powders synthesized by solid state reaction typically have an inversion parameter that is around 0.25.[14] Site inversion is difficult to detect using X-ray diffraction (XRD) due to the similar X-ray scattering cross sections for Mg (12) and Al (13). In contrast, the neutron scattering cross sections for Mg (0.06 barn) and Al (0.23 barn) are significantly different, which enables the use of neutron powder diffraction (NPD) to determine site occupancy.[15]

Mechanical activation is a high energy ball milling process that induces physical and chemical changes in materials.[6,7,16] Mechanical activation induces defects in materials that increase the chemical activity and potential energy of the activated material relative to equilibrium materials. This process can increase the speed of reactions and drastically decrease the reaction temperatures.[17] Mechanical activation can decrease processing time in that it can enable mixing and particle size reduction of constituents and, in some cases, solid-state reactions of a multicomponent system in a single process.[18]

The aim of the present study is to determine the influence of mechanical activation on site occupancy in the $MgAl_2O_4$ spinel (MAS).

2. EXPERIMENTAL PROCEDURE

2.1 PROCESSING

Magnesium oxide powder (≥99%, -325 mesh, Sigma-Aldrich) was heated in air at 10°C/min and calcined at 1000°C for 4 hours to decompose any hydroxide or carbonate species. The calcined MgO powder was then mixed with alumina powder (A16-SG, Almatis) by dry ball milling for 24 hours with ½" alumina media using a media to powder mass ratio of 1:1. After mixing, the precursor powder was ground using a pestle and mortar and sieved to 80 mesh. Approximately 12 grams of the mixed powder was mechanically activated (MA) using high energy ball milling (SPEX; Model No. 8000) with 5 mm alumina spherical media and an alumina mill jar. The media to powder mass ratio was approximately 3 to 1. The powder was milled for 60 minutes using a cycle of 30

minutes on, 15 minutes off, and then the final 30 minutes to reduce powder heating. After milling, the powder was passed through an 80-mesh sieve with minimal grinding.

Powders that were either as-mixed or mixed plus mechanically activated were loaded into alumina crucibles and reacted at temperatures from 1200°C to 1500°C for 2 hours in stagnant air (DT-30, Deltech, Colorado). The heating rate was 10°C/min and the furnace was allowed to cool at its natural rate after the isothermal hold. Powders were denoted as either mixed (XD) or mechanically activated (MA) along with the calcination temperature (e.g., MA1200C denotes mechanically activated powder calcined at 1200°C).

2.2 CHARACTERIZATION

Reacted powders were lightly ground using a mortar and pestle and sieved to -200 mesh for X-ray diffraction (XRD; X'Pert Pro, PANalytical, Almelo, NLD). Phase analysis of XRD data was performed by Rietveld refinement (RIQAS4, Materials Data Incorporated, Livermore, USA). Phases were modeled using the appropriate ICSD data. Powder morphologies were examined by scanning electron microscopy (SEM; Raith eLine, Raith GmbH, Islandia, New York). Powders were coated with a conductive Au/Pd layer before SEM.

Neutron diffraction patterns were collected on POWGEN at ORNL through the mail-in program.[19] The average sample mass was 1.5 g, which was loaded into vanadium sample cans. Collection time per sample was, on average, 3300 s for a proton charge of 4.5×10^{12} C. The central wavelength was 1.5 Å, which was used to assess lattice spacings from 0.485 Å to 13 Å. The total number of refined diffraction peaks was 133 per sample.

Rietveld refinement was done using GSAS-II.[20] As a starting point for the refinement, the Crystallographic Information File (CIF) from Yamanaka et al. was used assuming a site occupation of 100% Al and 0% Mg on 16c (octahedral position) and 100% Mg and 0% Al on 8b (tetrahedral position).[21] The first step in the refinement was to scale calculations to the experimental values. Shape parameters were refined using a pseudo-Voigt with Gaussian and Lorentzian parameters. The Lorentzian parameters were not refined as sample effects were captured in the Gaussian portion. The background was described using a Chebyshev polynomial since it is not constant over the Q-range. For the unit cell, only the a-axis lattice parameters were refined as no obvious reduction in symmetry occurred. The oxygen fractional coordinates and isotropic displacement were also refined. The second step of the refinement allowed the occupied site fractions for the 16c and 8b to vary with the isotropic displacement parameter. The isotropic thermal motion parameters (U_{iso}) on a specific site were constrained to be equal for Al and Mg. The specific site was constrained to be fully occupied (Al1+Mg2=1, Al2+Mg1=1). Both parameters are heavily correlated with Mg, Al occupancy. Further, site occupancy could not be refined without these constraints or the restrains in the next paragraph.

The chemical composition target was 8 Mg and 16 Al per unit cell with a restrain weight factor of 150. If the initial assumption for the weight factor were too high, the refinement would stay at the initial configuration without changing the site occupancy. If the initial assumption for the weight factor were too low, then the chemical composition deviated to become Mg deficient and Al rich. The weight factor was manually adjusted to keep the nominal Mg content per unit cell to 8.00 ± 0.05 atoms for all refinements. The procedure described herein enabled optimization of all fitting parameters in the first step

and then site occupancy in the second step. This refinement procedure was reproducible in contrast to sequential fitting methods that resulted in different site occupation with each iteration.

3. RESULTS & DISCUSSION

Heating the mixed or mechanically activated precursor powders to 1200°C, 1300°C 1400°C and 1500°C produced crystalline $MgAl_2O_4$. Analysis of the XRD patterns (Figure 1) for XD and MA powders confirmed that each specimen contained a single phase that indexed to $MgAl_2O_4$ (PDF: 01-074-1133) without any detectable residual MgO or Al_2O_3, or other impurity phases. All of the calcining temperatures chosen for this study were able to fully convert the precursor powders to crystalline $MgAl_2O_4$.

As with the XRD results, the neutron diffraction patterns of both the XD and MA materials indexed to the spinel structure. Figure 2 shows the neutron diffraction pattern of XD1500C, which is representative of the patterns collected for all of the materials in this study. Table 1 contains the peak listings of the main peaks indexed to the spinel structure. As seen in Figure 2, only peaks from a time of flight (TOF) of about 30000 μs and larger are labeled with Miller indices. The labeled peaks were enough to show that the NPD pattern was consistent with spinel formation, but higher order planes were too close to one another to label in this format. The most intense peak was at a TOF of roughly 32255 μs corresponds to the (440) plane. The next most intense peak was at approximately 45631 μs and was attributed to the (400) plane. The peak from the (222) plane was the

third most intense peak as was at a TOF of about 52692 µs. As with the XRD patterns, all of the NPD patterns were consistent with the formation of single-phase $MgAl_2O_4$.

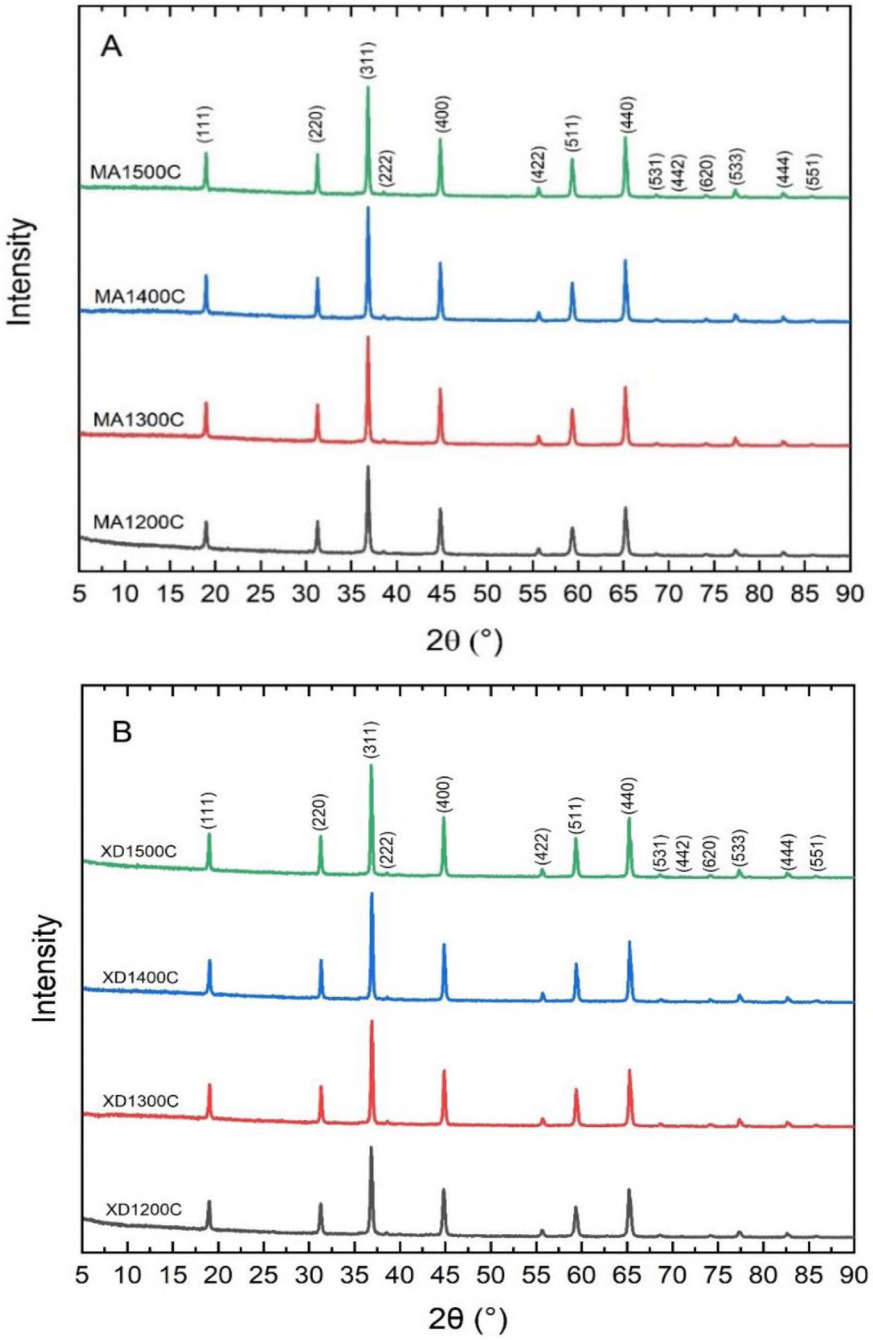

Figure 1. XRD patterns of the heat-treated MA (A) and XD (B) powders

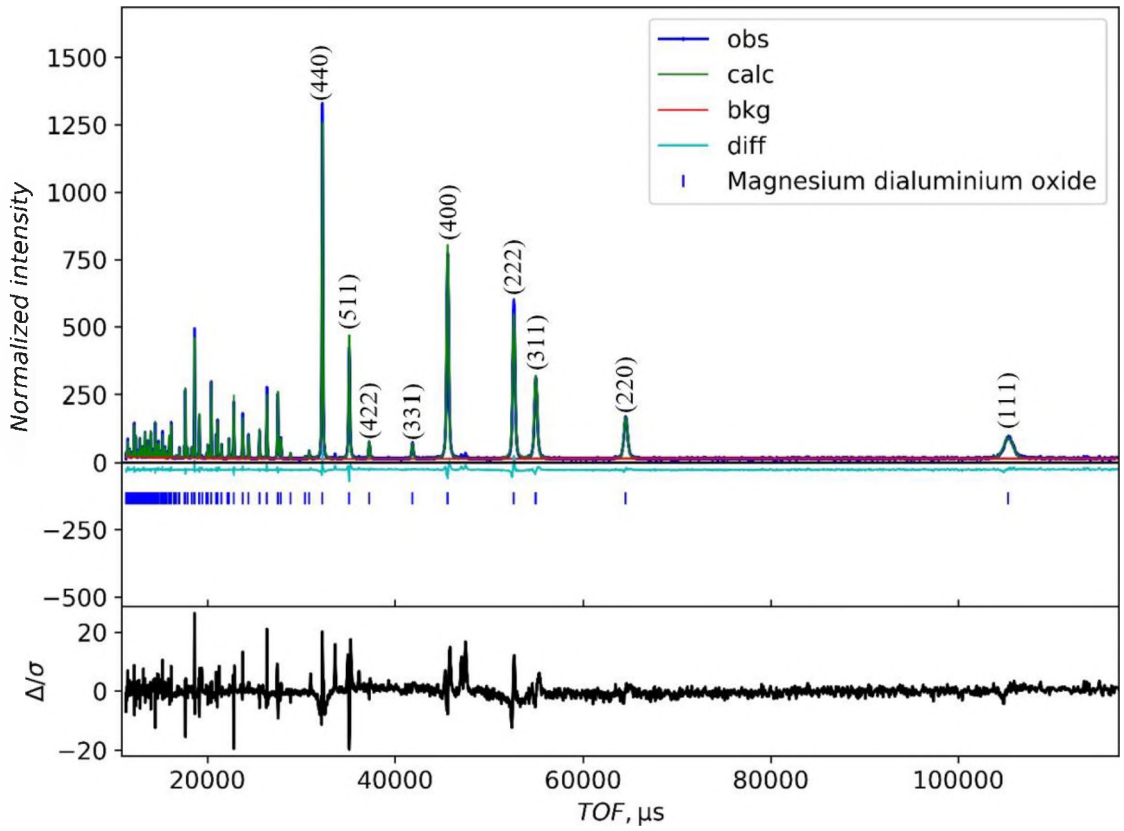

Figure 2. Representative neutron diffraction pattern for XD1500C with the Rietveld refinement fit.

Table 1. Peak listing of sample XD1500C displayed in Figure 2.

TOF (µs)	d-spacing (Å)	Miller Indice	RI (%)
105287	4.6677	*111*	7.27
64554.0	2.8584	*220*	13.23
55060.7	2.4376	*311*	23.81
52692.5	2.3339	*222*	42.17
45631.5	2.0212	*400*	58.99
41924.3	1.8548	*331*	4.90
37246.8	1.6503	*422*	6.49
35135.6	1.5559	*511*	34.54
32255.5	1.4292	*440*	100.00

The fractions of 16c and 8b sites occupied by Mg and Al were refined with isotropic displacement parameters for each powder. Each of the 133 diffraction peaks that were observed were used in each of the refinements. An impurity phase indicated by two small peaks was detected by NPD that was not detected by XRD. This impurity phase is likely residual MgO and/or Al_2O_3 and was not included in the refinement. In Table 2, the results of the refinement are shown, the R factor below 3% indicates a good refinement[22], the Al1 and Mg2 columns correlate to the site occupancy of the 8b or tetrahedral position in the spinel structure. Based on the refinement, XD1500C was determined to have an inversion parameter of $i = 0.13$, which was the lowest inversion parameter of the NMA materials.

The Mg1 and Al2 columns correspond to the site occupancy of the 16c or octahedral position in the spinel structure. As stated above, the refinements were set so that each site was fully occupied i.e., Al1+Mg2 = 1 and Al2+Mg1=1. The last column labeled "Mg" is the number of Mg atoms per unit cell after refinement. The weight factor was manually adjusted to keep this deviation ±0.05 from the nominal composition of 8 Mg atoms per unit cell. The Rietveld refinement produced results that have similarities with previous work on site occupancy and mechanical activation, which will be discussed in greater detail in the next section.

The site occupancy data from Table 2 is summarized in Figure 3. Starting from the top, the XD1200C material, returned with the largest cation disorder or inversion parameter of 0.185. The next material studied, XD1300C, has an inversion parameter $i = 0.149$, significantly lower than the XD1200C sample. This trend of decreasing inversion value as calcination temperature increases continues with the next two samples,

XD1400C and XD1500C having inversion parameter values of 0.132 and 0.130, respectively. All of the mixed powders had inversion parameters of at least 0.13 with inversion decreasing as calcining temperature increased. The decrease in inversion parameter with increasing calcination temperature is thought to be due to the higher mobility of the cations at higher temperatures allowing the cations to shift to their equilibrium positions.

Table 2. The table shows the site occupation in percent. Al2 and Mg1 are on 16c, Mg2 and Al1 are on 8b. Standard crystallographic cell Wyckoff sequence ecb.

Designation	Phase RF/RF^2 (%)	Al1 (%)	Mg2 (%)	Mg1 (%)	Al2 (%)	Mg
XD1200C	2.46/3.93	18.53	81.47	9.14	90.86	7.98
XD1300C	2.36/3.53	14.98	85.02	7.44	92.56	7.99
XD1400C	2.45/3.98	13.19	86.81	6.45	93.55	7.98
XD1500C	2.66/3.88	13.02	86.98	6.33	93.67	7.97
MA1200C	2.59/4.14	12.37	87.63	5.98	94.02	7.97
MA1300C	2.62/4.47	7.47	92.53	3.48	96.52	7.96
MA1400C	2.67/4.44	7.41	92.59	3.45	96.55	7.96
MA1500C	2.78/4.29	9.72	90.28	4.69	95.31	7.97

The mechanically activated powders did not show a clear trend with temperature. The inversion parameter was about 0.124 for MA60-1200C. The MA60-1300C and MA-1400C samples each had lower values of cation site disorder with values of i=0.075 for MA60-1300C and 0.074 for MA60-1400C. In contrast, increasing the calcining

temperature to 1500°C for MA60-1500C led to an increase in the inversion parameter to 0.097. As with the XD powders, the decrease in inversion parameter when calcination temperature increased from 1200°C to 1400°C was thought to be due to same mechanism that led to the decrease in inversion with increasing calcination temperature in the XD powders, which is increased cation mobility with increasing temperature. The increase in inversion parameter for the 1500°C is thought to be due to a competing mechanism that increases cation disorder. While increasing temperature increases mobility and allows cations to move to their equilibrium positions, higher temperatures also promote disorder through the increase in entropy with increasing temperature.

Regardless of temperature, the inversion parameters for the MA materials were all lower than the lowest inversion value for the XD samples. Mechanical activation is known to produce defects in powder particles that results in a higher energy state compared to the non-activated powders. Our hypothesis is that this higher energy starting state allows the MA powders to get closer to equilibrium than the XD powders for the same heat treatment temperature. These results generally agree with a previous study by Obradovic et al. who used Raman spectroscopy to characterize cation inversion in mechanically activated spinel powders.[23] Whereas Obradovic et al. found that inversion decreased with increasing temperature for activated materials, the present study reveals that this is true, but may be reversible upon reaching a temperature threshold. The investigation by Obradovic et al. also found lower inversion for mechanically activated materials at some temperatures, the present work revealed that all activated materials had lower degrees of inversion than the mixed powders. The differences in trends may be due to the measurement methods. Raman is more sensitive to the surface of powder particles

compared to neutron powder diffraction, which penetrates through the powder particles and is a true bulk measurement. Overall, the MA had lower inversion parameters than the XD powders. In addition, both calcination temperature and mechanical activation have an effect on cation site disorder and thus the inversion parameter. Further investigation is necessary to determine if calcination temperatures above 1500°C will produce material with greater cation site disorders than observed here.

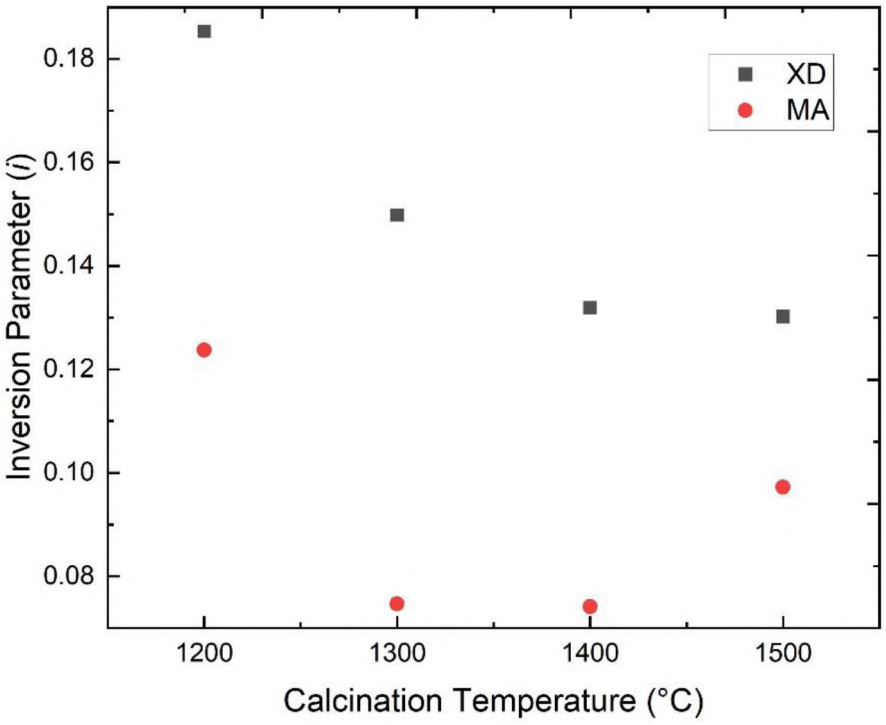

Figure 3. Inversion parameter vs. calcination temperature plotted for the spinel powders.

4. SUMMARY

The crystallographic site occupancy of stoichiometric $MgAl_2O_4$ powders were studied to determine the effect of temperature and mechanical activation on the cation site occupancy. Heating the various powders to at least 1200°C produced single phase $MgAl_2O_4$ spinel powders, with or without mechanical activation, which was confirmed by both XRD and neutron diffraction analysis. The mechanically activated $MgAl_2O_4$ powders had lower degrees of inversion than the lowest inversion parameter for mixed powders. The relationship between temperature and the degree of inversion indicates that competing mechanisms affect cation site occupancy. The lower inversion in MA powders compared to XD powders was attributed to the higher energy state of the MA powders prior to calcination that provided a higher driving force to approach equilibrium (i.e., zero inversion) at the same calcining temperature. In addition, higher calcining temperatures appear to increase atom mobility and allow for lower degrees of inversion, but higher calcining temperatures can also result in more thermally-activated site disorder. More research into how mechanical activation and temperature affect cation site disorder is needed to determine the mechanisms at play here.

ACKNOWLEDGEMENTS

This research was partially funded by the Enabling Materials for Extreme Environments signature area at Missouri S&T. The research used resources at the Spallation Neutron Source, a DOE Office of Science User Facility operated by the Oak Ridge National Laboratory. The authors would like to thank the Advanced Materials

Characterization Lab at Missouri S&T for use of the characterization equipment. C.C. would also like to thank the ultra-high temperature ceramics group at Missouri S&T for the sound advice and help completing research tasks.

REFERENCES

1) Ianoş R, Lazău I, Păcurariu C, Barvinschi P. Solution combustion synthesis of $MgAl_2O_4$ using fuel mixtures. *Mater Res Bull*. 2008;43(12):3408–3415. https://doi.org/10.1016/j.materresbull.2008.02.003.

2) Esposito L, Piancastelli A, Martelli S. Production and characterization of transparent $MgAl_2O_4$ prepared by hot pressing. *J Eur Ceram Soc*. 2013;33(4):737–747. https://doi.org/10.1016/j.jeurceramsoc.2012.10.013.

3) Obradovic N, Fahrenholtz W, Filipovic S, *et al.* Characterization of MgAl2O4 sintered ceramics. *Sci Sinter*. 2019;51(4):363–376. https://doi.org/10.2298/SOS1904363O.

4) Obradović N, Fahrenholtz WG, Filipović S, *et al.* The effect of mechanical activation on synthesis and properties of $MgAl_2O_4$ ceramics. *Ceram Int*. 2019;45(9):12015–12021. https://doi.org/10.1016/j.ceramint.2019.03.095.

5) Reimanis I, Kleebe HJ. A review on the sintering and microstructure development of transparent spinel ($MgAl_2O_4$). *J Am Ceram Soc*. 2009;92(7):1472–1480. https://doi.org/10.1111/j.1551-2916.2009.03108.

6) Sokol M, Halabi M, Kalabukhov S, Frage N. Nano-structured $MgAl_2O_4$ spinel consolidated by high pressure spark plasma sintering (HPSPS). *J Eur Ceram Soc*. 2017;37:755–762. https://doi.org/10.1016/j.jeurceramsoc.2016.09.037.

7) Kosanović D, Labus NJ, Živojinović J, Tadić AP, Blagojević VA, Pavlović VB. Effects of mechanical activation on the formation and sintering kinetics of barium strontium titanate ceramics. *Sci Sinter*. 2020;52(4):371–385. https://doi.org/10.2298/SOS2004371K.

8) Ye G, Troczynski T. Mechanical activation of heterogeneous sol-gel precursors for synthesis of $MgAl_2O_4$ spinel. *J Am Ceram Soc*. 2005;88(10):2970–2974. https://doi.org/10.1111/j.1551-2916.2005.00533.

9) Dwibedi D, Avdeev M, Barpanda P. Role of Fuel on Cation Disorder in Magnesium Aluminate ($MgAl_2O_4$) Spinel Prepared by Combustion Synthesis. *J Am Ceram Soc*. 2015;98(9):2908–2913. https://doi.org/10.1111/jace.13705.

10) R. J . Bratton. Co-precipitates yielding $MgAl_2O_4$ spinel powders. *American Ceramic Society Bulletin,* 48(8):759-762, 1969.

11) Li JG, Ikegami T, Lee JH, Mori T, Yajima Y. A wet-chemical process yielding reactive magnesium aluminate spinel ($MgAl_2O_4$) powder. *Ceram Int*. 2001;27(4):481–489. https://doi.org/10.1016/S0272-8842(00)00107-3.

12) O'Quinn EC, Shamblin J, Perlov B, *et al.* Inversion in $Mg_{1-x}Ni_xAl_2O_4$ Spinel: New Insight into Local Structure. *J Am Chem Soc*. 2017;139(30):10395–10402. https://doi.org/10.1021/jacs.7b04370.

13) Torruella P, Ruiz-Caridad A, Walls M, *et al.* Atomic-Scale Determination of Cation Inversion in Spinel-Based Oxide Nanoparticles. *Nano Lett*. 2018;18(9):5854–5861. https://doi.org/10.1021/acs.nanolett.8b02524.

14) Sickafus KE, Wills JM, Grimes NW. Structure of spinel. *J Am Ceram Soc*. 1999;82(12):3279–3292. https://doi.org/10.1111/j.1151-2916.1999.tb02241.

15) Toby BH. NIST Center for Neutron Research. 2001;106(6):965–973.

16) Abdi MS, Ebadzadeh T, Ghaffari A, Feli M. Synthesis of nano-sized spinel ($MgAl_2O_4$) from short mechanochemically activated chloride precursors and its sintering behavior. *Adv Powder Technol*. 2015;26(1):175–179. https://doi.org/10.1016/j.apt.2014.09.011

17) Popova NA, Lukin ES, Pavlyukova LT, Sevostyanov MA, Leonov A V. Synthesis of alumomagnesian spinel by mechanical activation method. *IOP Conf. Ser. Mater. Sci. Eng.* Vol. 525. 2019 https://doi.org/10.1088/1757-899X/525/1/012071.

18) Tavangarian F, Li G. Mechanical activation assisted synthesis of nanostructure $MgAl_2O_4$ from gibbsite and lansfordite. *Powder Technol*. 2014;267:333–338. https://doi.org/10.1016/j.powtec.2014.08.003.

19) Huq A, Kirkham M, Peterson PF, *et al.* POWGEN: Rebuild of a third-generation powder diffractometer at the Spallation Neutron Source. *J Appl Crystallogr*. 2019;52:1189–1201. https://doi.org/10.1107/S160057671901121.

20) Toby BH, Von Dreele RB. GSAS-II: The genesis of a modern open-source all-purpose crystallography software package. *J Appl Crystallogr*. 2013;46(2):544–549. https://doi.org/10.1107/S0021889813003531.

21) YAMANAKA T. Thermal Movement of Atoms in the Spinel Structure. *J Mineral Soc Japan*. 1983;16(2):221–231. https://doi.org/10.2465/gkk1952.16.221.

22) Toby, B. (2006). R factors in Rietveld analysis: How good is good enough? *Powder Diffraction, 21*(1), 67-70. doi:10.1154/1.2179804.

23) Obradović N, Fahrenholtz WG, Filipović S, *et al.* Formation kinetics and cation inversion in mechanically activated $MgAl_2O_4$ spinel ceramics. *J Therm Anal Calorim*. 2020;140(1):95–107. https://doi.org/10.1007/s10973-019-08846-w/.

II. SYNTHESIS AND CHARACTERIZATION OF A HIGH ENTROPY SPINEL

Cole A. Corlett[1], N. Obradovic[2], Jeremy L. Watts[1], William G. Fahrenholtz[1]

[1]Missouri University of Science & Technology, Rolla, MO, USA

[2]Institute of Technical Sciences of SASA, Knez Mihailova 35/IV, 11000 Belgrade, Serbia

ABSTRACT

The synthesis, densification behavior, and crystallographic site occupancy were investigated for four spinel-based ceramics, including a high-entropy spinel $(Co_{0.2}Cu_{0.2}Mg_{0.2}Ni_{0.2}Zn_{0.2})Al_2O_4$. Each composition reacted to form a single phase, but analysis of X-ray diffraction patterns revealed differences in cation site occupancy. Densification behavior was investigated and showed that fully dense ceramics could be produced by hot pressing at temperatures as low as 1375°C for all compositions. Vickers hardness values were found to be 10 GPa and higher for all compositions. This is the first study to synthesize and characterize the high-entropy aluminate spinel material $(Co_{0.2}Cu_{0.2}Mg_{0.2}Ni_{0.2}Zn_{0.2})Al_2O_4$.

1. INTRODUCTION

Magnesium aluminate, $MgAl_2O_4$, which is commonly referred to by its mineral name of spinel, is the only compound in the MgO-Al_2O_3 binary system. Interest in spinel ceramics is driven by properties such as high melting point (> 2100 °C), high hardness (~

13 GPa), resistance to chemical attack, and the potential for optical transparency.[1-3] These exceptional properties are what allow spinel ceramics to be used in applications such as catalyst-supports, refractories, transparent armor, and radiation tolerant ceramics.[4,5] Several methods can be used to fabricate spinel-based ceramics, including direct solid-state reactions, wet chemical techniques and mechanical activation techniques.[7-14]

2. EXPERIMENTAL PROCEDURE

Raw materials were batched to produce spinel powders with different compositions. Prior to batching, magnesium oxide powder (≥99%, Sigma-Aldrich) was first calcined in air at 1000 °C for 4 hours with a heating rate of 10 °C/min to decompose any carbonate, hydroxide, and/or hydroxycarbonate species to oxides. To produce the magnesium aluminate spinel, $MgAl_2O_4$, (MAS), calcined magnesium oxide and α-Al_2O_3 (A16-SG Almatis) were mixed in a one-to-one molar ratio by ball milling for 24 hours in acetone. Likewise, nickel aluminate spinel, $NiAl_2O_4$ (NAS), was synthesized by mixing NiO (78.5% Ni, Alfa Aesar) and Al_2O_3 in a one-to-one molar ratio by ball milling for 24 hours in acetone. A mixed, nickel-magnesium aluminate spinel, $(Mg_{0.5},Ni_{0.5})Al_2O_4$, (NMAS) was produced by mixing equimolar amounts of calcined MgO and NiO with one molar equivalent of α-Al_2O_3 by ball milling for 24 hours in acetone. To produce the high entropy spinel (HES), one molar equivalent of α-Al_2O_3 was mixed with the appropriate amounts of calcined MgO, NiO, ZnO (99.9%, Alfa Aesar), CuO (97%, Alfa Aesar), and Co_3O_4 (99.7%, Alfa Aesar) by ball milling for 24 hours in acetone. The target composition was $(Co_{0.2}Cu_{0.2}Mg_{0.2}Ni_{0.2}Zn_{0.2})Al_2O_4$.

Once the powders were mixed for 24 hours, the slurries were dried by rotary evaporation (Rotovapor R-124; Buchi, Flawil, DEU). The subsequent powers were lightly ground to break large agglomerates and passed through an 80-mesh screen. After sieving, the powders were mechanically activated (MA) by high energy ball milling (Model No. 8000, Spex Industries, Inc.) with a cycle of 30 minutes on, 15 minutes off, and then the final 30 minutes for a total 60 minutes of active milling. The off time was added to minimize powder heating. Powders were loaded into an alumina mill jar with 5 mm alumina spherical media in increments of 12 grams of powder with a media to powder mass ratio of 3:1. After milling, the powder mixtures were pushed through an 80-mesh screen. At this point, the milled powder mixtures were loaded into alumina crucibles and reacted at 1200°C for 2 hours in a box furnace (Deltech, Colorado) in static air.

Dense HES ceramics were prepared by reactive hot pressing (RHP) in a 25.4 mm diameter graphite die lined with graphite paper (0.005"; Graftech International, Lakewood, USA) and coated with BN (SP-108; Materion, Milwaukee, USA). A tungsten metal sheet that was coated on both sides with BN was placed between the graphite paper and the powder compact to minimize carbon diffusion into the specimens. Densification data were collected by measuring ram displacement using a linear variable differential transducer (LVDT) and analyzed using OriginLab graphical software. The hot press (HP; Model HP20-3060-20; Thermal Technology, Santa Rosa, USA) was heated under flowing argon at 25°C/min to 1150°C and then 10°C/min to 1200°C with a 2 hour hold at 1200°C to allow the oxide precursors to react. After the 2-hour hold, a uniaxial load of 32 MPa was applied, and the furnace heated at a rate of 25°C/min to 50°C below the final

hold temperature. It was at this point that data collection for densification began. The furnace was then heated at 10°C/min to the final hold temperature of either 1375°C, 1450°C or 1550°C and was held for 30 minutes. The furnace was allowed to cool at 10°C/min from the final hold temperature to 1200°C, at which point the load was removed and the furnace was allowed to cool at its natural rate. Specimens were surface ground to remove the tungsten sheet and any reaction layer. A modified Archimedes method was then used to measure the bulk density of each hot-pressed billet. The billets were then cross sectioned and polished to a 0.25 μm finish using successively finer diamond abrasives.

Reacted powders were ground and passed through an 80-mesh screen prior to X-ray diffraction analysis (XRD; X'Pert Pro, PANalytical, Almelo, NLD). Phase analysis was performed by Rietveld refinement (RIQAS4, Materials Data Incorporated, Livermore, USA). Phases were modeled using Inorganic Crystal Structure Database (ICSD) card 01-071-0965 for $MgAl_2O_4$, card 01-071-0865 for $NiAl_2O_4$ and $(Mg_{0.5},Ni_{0.5})Al_2O_4$, and card 01-075-1605 for $(Co_{0.2}Cu_{0.2}Mg_{0.2}Ni_{0.2}Zn_{0.2})Al_2O_4$. Lattice parameters determined using Rietveld refinement of XRD data were used to calculate the theoretical density of the HES material assuming a cubic crystal structure and a space group number of $F\bar{4}3m$. Rietveld refinement was also used to estimate site occupancies for the various cation sites to determine the amount of inversion (i.e., occupancy of Mg sites by Al cations). An initial refinement was performed for each material to get close to the site occupancy values for each material. Once that was done, refinements were performed by inputting specific occupancy values to determine where the site occupancy and fit error values converged. Precursor powders were analyzed for specific surface area

(SSA) using the Brunauer-Emmett-Teller (BET) method (NOVA 2000e; Quantachrome Instruments, Boynton Beach, FL). Equivalent particle size was calculated by assuming that particles had a spherical shape. Calculated true densities (ρ) of each powder were also used in the calculation.

$$d = \frac{6}{SSA \cdot \rho} \quad (1)$$

Morphologies of both precursor and reacted powders were examined by scanning electron microscopy (SEM; Raith eLine, Raith GmbH, Islandia, New York). Powders were coated with a conductive Au/Pd coating before placing into SEM. Microhardness (H_v) was measured with a Vickers' diamond indenter (Duramin-5, Struers, Cleveland, OH), with 10 indents performed for each reported value. Phase analysis of polished sections of hot-pressed billets was performed using XRD.

3. RESULTS AND DISCUSSION

Heating to 1200°C produced crystalline MAS. Analysis of the XRD pattern (Figure 1) revealed that the specimen contained a single spinel phase (PDF: 01-077-0435) and all peaks indexed to MAS with no other peaks present. The lattice parameter obtained for the MAS material was 8.08410 ± 0.00004 Å based on the Rietveld refinement fit (Table 1). The calculated true density using the nominal composition and the measured lattice parameter was 3.58 g/cm^3, which agrees with previous reports.[4] The first several peaks of the MAS material were similar to the card to which it was indexed. Table 2 summarizes the XRD information with peak location and relative intensities. The peak located at roughly 19° for the (111) peak had a relative intensity (RI) of about 38%,

which is comparative to 39.4% from the card. The (220) peak at ~31.2° had a RI of 33.5% but the XRD analysis revealed a RI of about 37.7% from the present study. The (311) peak at 36.8° was the 100% intensity peak for both the present material and the XRD card. The (222) peak at 38.5° was significantly lower in relative intensity than the previous peaks at 4.8% for this study and 0.9% from the PDF card. Another example of a peak with a difference in RI is the (511) peak at 59.3°. The card lists a RI of 40.1% and the present material only had an RI of 34.4%. For MAS, the peak positions were all nominally the same as listed on the PDF card, but differences in relative intensities were observed that may be due to partial inversion of the structure or other factors.

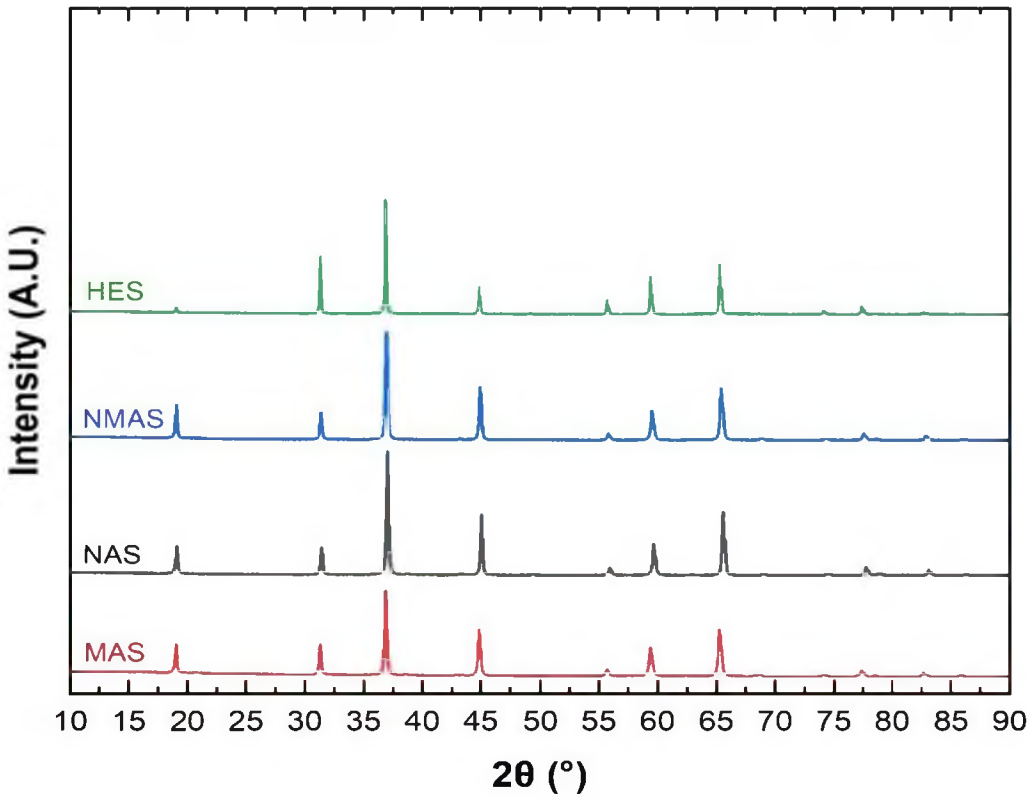

Figure 1. XRD patterns of reacted spinel powders.

Heating the NAS and NMAS materials to 1200°C produced crystalline spinel materials. Analysis of the XRD patterns (Figure 1) revealed that the specimens were each composed of a single spinel phase (PDF: 01-081-0721 - NAS; 01-071-0965 - NMAS). Each peak was indexed to the respective card with no additional peaks present, which is summarized in Table 1. The lattice parameters from the Rietveld refinements were 8.04839 ± 0.00005 Å for NAS and 8.06751 ± 0.00004 Å for NMAS. The theoretical densities calculated from the measured unit cell parameters and the nominal compositions were 4.50 g/cm^3 for NAS and 4.03 g/cm^3 for NMAS. The calculated value for NAS agrees with the accepted density of 4.51 g/cm^3 and the density for NMAS is consistent with the composition since lighter Mg atoms replace half of the Ni atoms in the structure. The relative intensities of the peaks of NAS match well with those listed on the PDF card used to index the pattern. Some small differences were noted, such as the (220) peak 31.4° and the (222) peak at 38.8° which had higher relative intensities than listed on the PDF card. For the other peaks, the measured relative intensities were consistent with the values listed on the PDF card. As with NAS, the relative intensities of the NMAS peaks match well with the PDF card, with some noticeable differences for a few key peaks. The first noted difference was the (111) peak located at about ~19° that had a measured RI of 36.8% whereas the card lists an RI of 19.9%. The next two peaks, the (220) peak at 31.3° and the (311) peak at 36.8°, both match well with the peak intensities listed on the card, but the fourth peak diverges again. The card shows a peak intensity of 1.1% at for the (222) peak at 38.7° but the measured relative intensity was nearly 7%. These differences may be due to the composition since the card used to index NMAS is actually $NiAl_2O_4$ and not the same composition as the NMAS material studied.

Table 1. Indexed peaks of the four spinel materials. RI is relative intensity.

	MAS		NAS		NMAS		HES	
Plane	**Peak Position (2θ°)**	**RI (%)**	**Peak Position (2θ°)**	**RI (%)**	**Peak Position (2θ°)**	**RI (%)**	**Peak Position (2θ°)**	**RI (%)**
111	19.0	38.0	19.1	28.5	19.1	36.8	19.1	12.7
220	31.3	37.7	31.4	27.2	31.4	30.1	31.3	51.8
311	36.9	100.0	37.0	100.0	37.0	100.0	36.9	100.0
222	38.6	4.8	38.8	8.4	38.7	6.9	38.9	8.2
400	44.9	55.2	45.0	52.3	44.9	52.1	44.9	29.2
331	49.0	1.8	49.3	7.9	49.5	18.2	49.3	8.2
422	55.7	8.9	55.9	12.0	55.8	11.7	55.7	18.7
511	59.4	34.4	59.7	30.1	59.5	31.6	59.4	37.6
440	65.3	54.8	65.8	54.1	65.4	51.3	65.3	47.7
531	68.7	3.2	69.0	8.4	68.8	8.0	69.4	7.6
442	69.8	1.2	70.0	6.7	70.8	6.0	71.0	7.9
620	74.2	2.8	74.5	8.3	74.3	5.0	74.2	10.6
533	77.4	7.5	77.8	12.8	77.6	11.7	77.4	14.0
622	78.4	1.7	78.8	8.6	78.6	7.0	78.7	8.0
444	82.7	5.2	83.1	10.6	82.9	9.6	82.7	9.3
551	85.8	2.3	86.2	7.2	86.2	6.4	86.1	7.7

Heating to 1200°C was sufficient to produce a crystalline high entropy spinel. Analysis of the XRD pattern (Figure 1) showed that the specimen contained a single phase that could be indexed to the spinel structure of $CuAl_2O_4$ (PDF card 01-078-1605) with no additional peaks present. The calculated lattice parameter was 8.08307 ± 0.00004 Å with an estimated true density of 4.33 g/cm^3. The positions of the peaks present in the HES material matched well with the card used to identify the structure of the material. The (111) peak at 19° had a relative intensity of 12.7%, whereas the peak on the card only had a relative intensity of 2.2%. The (220) peak at 31.3° and the (311) peak at 36.9° had very similar relative intensities to those listed on the card, but the (222) peak at about

39° had an RI of 8.2% but the card lists an intensity of only 0.2%. The differences in relative intensity are likely due to the presence of the different cations in the A and B sites in the lattice as well as the site occupancy in the structure.

Rietveld refinement was used to estimate the site occupancies of the cations in the spinel structure for the various powders. Table 2 summarizes the site occupancies from the best fits along with predicted lattice parameters and true densities for each composition. Rietveld refinement of XRD data was unable to provide unambiguous site occupancy for MAS because the X-ray scattering cross sections of Mg and Al are very similar (i.e., 12 for Mg and 13 for Al). The degree of site inversion for MAS typically ranges from 0.1 to 0.6, depending on processing routes.[24,25] In contrast, NAS is an inverse spinel that typically has all of the A lattice sites occupied by Al with the Ni occupying B lattice sites. Fit error values of about 5% or less were found for simulations that assumed full inversion for NAS, NMAS, and HES. Based on the Rietveld refinement and the varying peak intensities, NMAS, NAS, and HES all appear to have a high degree of inversion (i.e., they are nearly fully inverted).

Table 2. Summary of Rietveld refinement of the spinel powders.

Designation	**Degree of Inversion**	**R_{wp} (%)**	**a-axis $_{measured}$ (Å)**	**Theoretical Density (g/cm^3)**
MAS	N/A	N/A	8.08410 ± 0.00004	3.58
NAS	0.5	3.08	8.04839 ± 0.00005	4.50
NMAS	0.4	3.89	8.06751 ± 0.00004	4.03
HES	0.4	2.42	8.08307 ± 0.00004	4.33

Mechanical activation reduced the starting particle sizes of the powders and homogenized the constituents. Table 3 summarizes the specific surface area (SSA) for milled and unmilled precursor powders along with equivalent particle sizes calculated from SSA. The SSA of each of the powders increased significantly after milling. Each starting (i.e., mixed) powder had a surface area of approximately 6 m^2/g and the surface areas increased for the milled powders to the range of 7.0 – 7.5 m^2/g, which is an increase in SSA of approximately 20%. Examining powder morphology showed that the most noticeable difference between unmilled and milled powders was the absence of the particles in the milled powders (Figure 2). The circle in Figure 2a highlights a large particle that was ~1 μm in diameter in the unmilled powder. Similar large particles were commonly observed in mixed powders, but none were found in milled powders. Other than the presence of a small fraction of large particles, the starting powders appeared to be sub-micron in size with an irregular polygon shape and did not change appreciably after milling. These observations match with the measured SSA as seen in Table 2. Hence, mechanical activation led to reduction in the number of large particles, which presumably increased the reactivity of the material.\

Densification curves for the milled HES at three different temperatures are shown in Figure 3. All specimens reached >98% relative density as summarized in Table 4. The specimen sintered at 1375°C reached full density during the isothermal hold, but the other two reached full density well before the final hold temperature was reached. It should be noted that the specimen with the largest initial densification rate was the specimen sintered at 1375°C, which was a rate of 6.2 min^{-1}. The other two specimens had initial densification rates of 2.8 min^{-1} for sintering at 1450°C and 4.3 min^{-1} for sintering at

1550°C. Despite these differences in initial densification rates, all specimens reached relative densities of more than 98%.

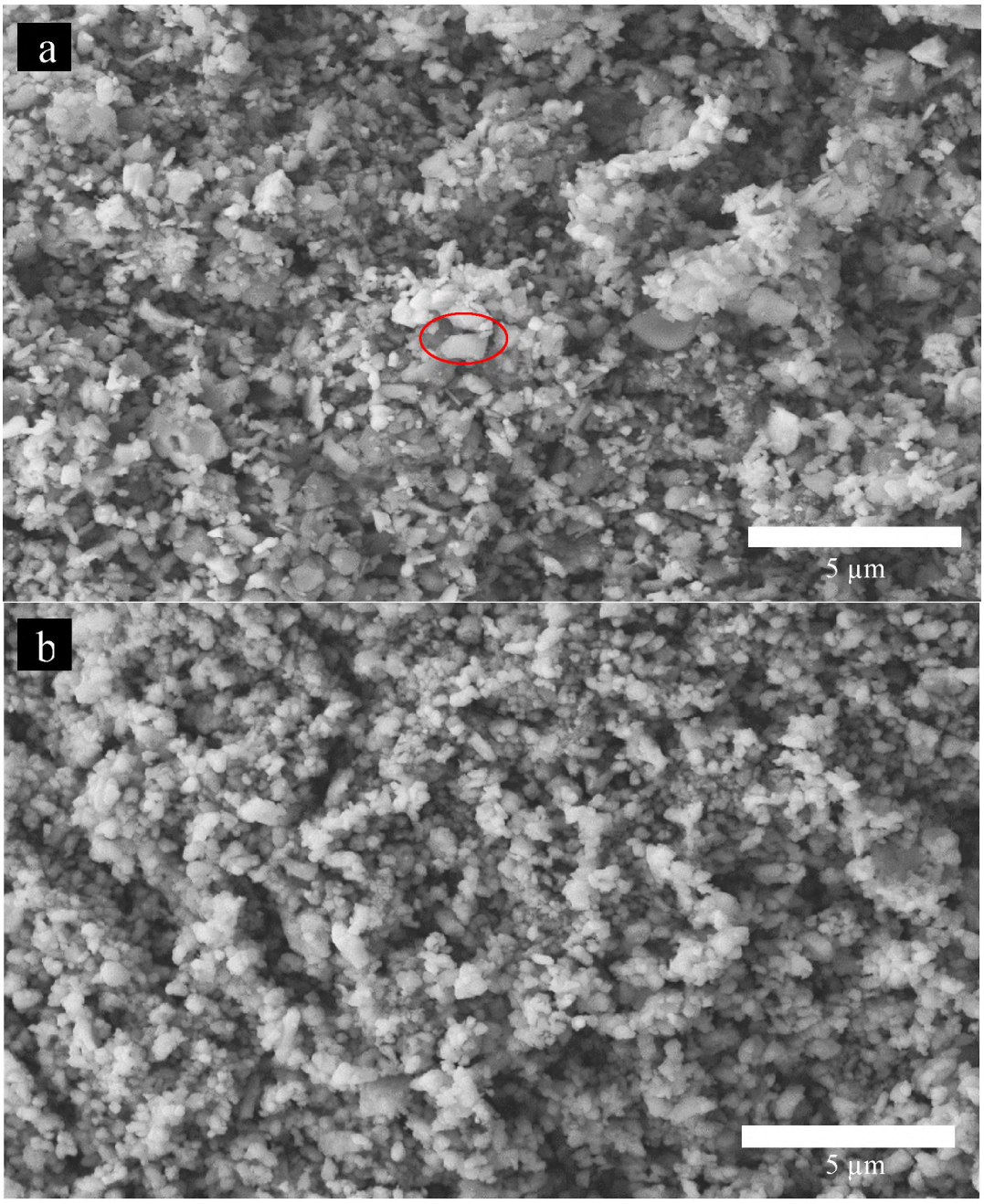

Figure 2. SEM micrographs of a) as-mixed b) milled HES powders after annealing at 1200 °C for 2 hours. The red circle highlights a larger particle present in the mixed material that is largely missing from the milled powder.

Table 3. Specific surface area and theoretical particle size of unreacted prepared powders.

Designation	Type	SSA (m^2/g)	SSA % Increase	Theoretical Particle Size (μm)
MAS	Unmilled	5.8	22	0.29
	Milled	7.0		0.24
NAS	Unmilled	5.6	52	0.24
	Milled	8.5		0.16
NMAS	Unmilled	5.9	20	0.25
	Milled	7.1		0.21
HES	Unmilled	6.0	23	0.23
	Milled	7.4		0.19

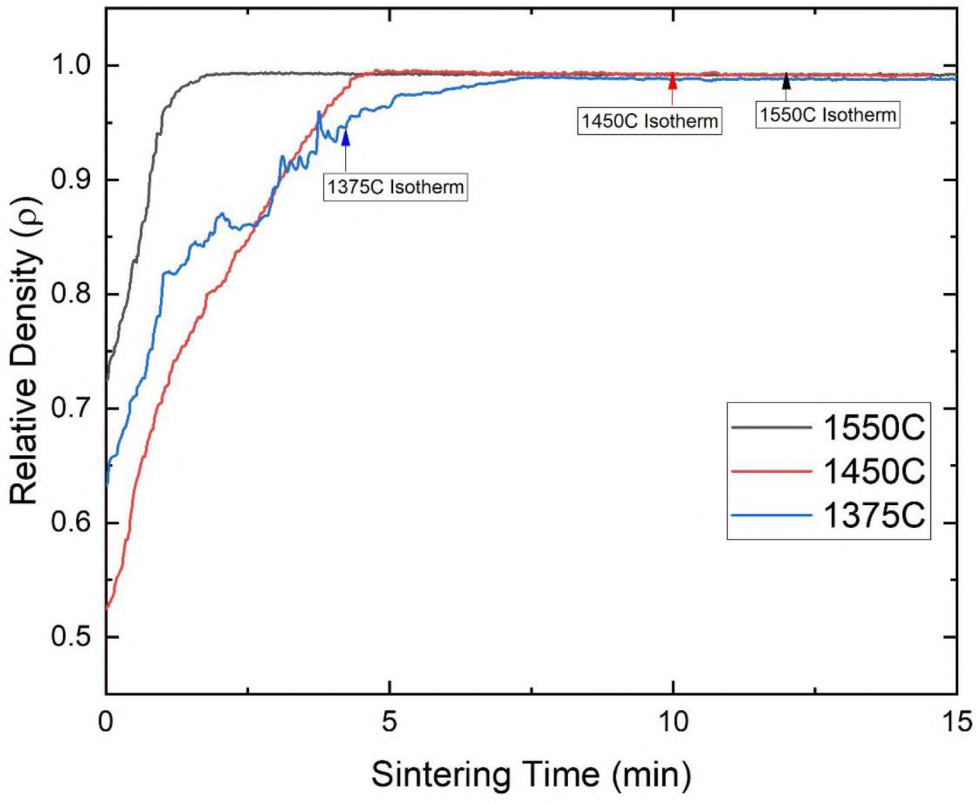

Figure 3. Relative density as a function of sintering time for HES powders. The sintering time begins when pressure was applied to the powder compacts. The vertical lines denote when the compacts reached the final sintering temperature.

Table 4. Densification rates and final densities for the three hot-pressed HES specimens.

Hold Temperature	Initial Densification Rate (min^{-1})	Bulk Density (g/cm^3)	Relative Density (%)
1375	6.2	4.27 ± 0.01	98.6 ± 0.2
1450	3.8	4.25 ± 0.01	98.0 ± 0.2
1550	4.3	4.29 ± 0.01	99.0 ± 0.1

Microhardness was measured for the hot-pressed materials at loads of 4.90 N and 9.81 N. These results along with the measured grain sizes are reported in Table 5 and a representative indentation can be seen in Figure 4. The indents were valid with no spalling noted and radial-median cracks appearing from the corners. The sample sintered at 1375°C had nearly the same hardness at each load with H_v of 14.1 ± 0.5 GPa at 4.90 N and 14.0 ± 0.5 GPa 9.81 N. The sample prepared at 1450°C had a hardness of 14.8 ± 0.4 GPa at 4.90 N and 13.3 ± 0.6 GPa at 9.8 N. The sample synthesized at 1550°C displayed similar hardness values as the 1450°C sample; 14.4 ± 0.4 and 13.2 ± 0.2 for the 4.90 and 9.21 N loads respectively. The values reported in the present study are comparable to previous reports such as Haney,[26] who reported hardness values of 14.1 GPa for coarse grained (250 μm) transparent MAS.

Table 5. Vickers hardness values and grain sizes for hot pressed HES samples.

Sintering Temperature (°C)	Load (N)	H_V (GPa)
1375	4.90	14.1 ± 0.5
	9.81	14.0 ± 0.5
1450	4.90	14.8 ± 0.4
	9.81	13.3 ± 0.6
1550	4.90	14.4 ± 0.4
	9.81	13.2 ± 0.2

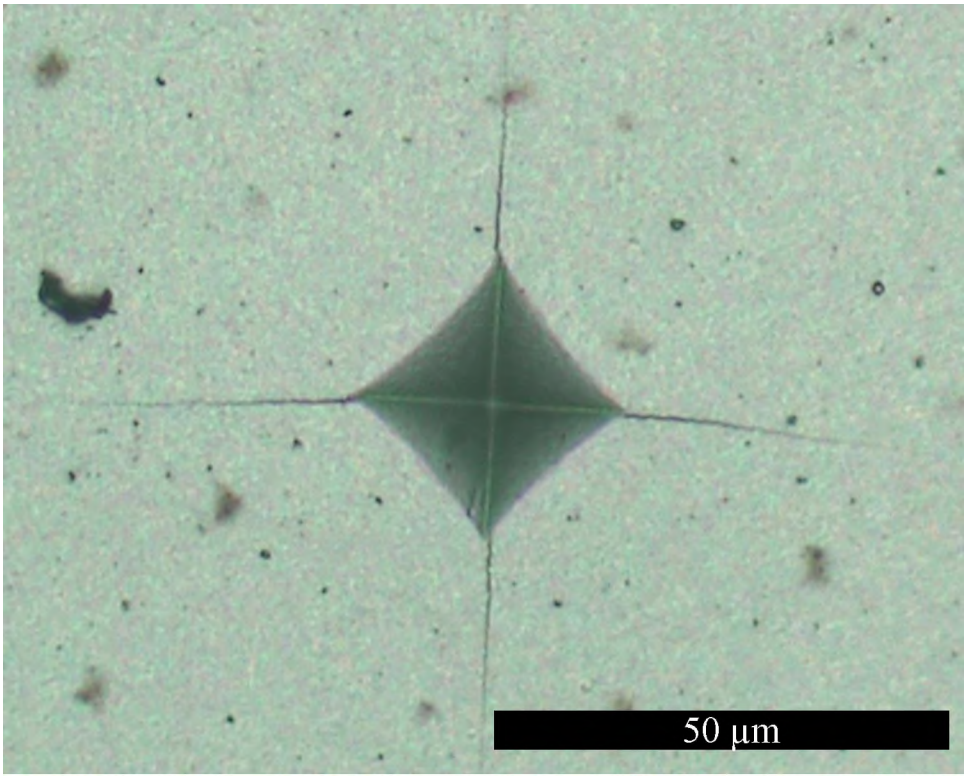

Figure 4. a) Representative Vickers indent of the hot pressed HES material sintered at 1375 °C b) representative image of grain size boundaries in HES material.

4. SUMMARY

This is the first report of the densification, site occupancy, and hardness of a high-entropy spinel. A spinel with the nominal composition of $(Co_{0.2}Cu_{0.2}Mg_{0.2}Ni_{0.2}Zn_{0.2})Al_2O_4$ and three other spinel materials were synthesized. The HES, NAS, and NMAS materials were all nearly fully inverse spinels, which was a much higher degree of cation inversion than MAS that was about 10% inverted. Mechanical activation increased the SSA of the powders by about 25% due to elimination of large particles from the mixture. Vicker's hardness values of the HES were all around 14 GPa, which is higher than hardness values reported for MAS at the same load. The research presented here serves to further the understanding of spinel and high-entropy oxide materials.

ACKNOWLEDGEMENTS

This research was partially funded by the Enabling Materials for Extreme Environments signature area at Missouri S&T. The authors would like to thank the Advanced Materials Characterization Lab at Missouri S&T for use of the characterization equipment and specifically Dr. Eric Bohannon for his assistance with XRD analysis. The UHTC group at Missouri S&T also deserves mentioned for the sound advice and help given in completing research tasks.

REFERENCES

1) Goldstein A, Goldenberg A, Yeshurun Y, Hefetz M. Transparent $MgAl_2O_4$ spinel from a powder prepared by flame spray pyrolysis. *J Am Ceram Soc*. 2008;91(12):4141–4144. https://doi.org/10.1111/j.1551-2916.2008.02788.

2) Ianoş R, Lazău I, Păcurariu C, Barvinschi P. Solution combustion synthesis of $MgAl_2O_4$ using fuel mixtures. *Mater Res Bull*. 2008;43(12):3408–3415. https://doi.org/10.1016/j.materresbull.2008.02.003.

3) Esposito L, Piancastelli A, Martelli S. Production and characterization of transparent $MgAl_2O_4$ prepared by hot pressing. *J Eur Ceram Soc*. 2013;33(4):737–747. https://doi.org/10.1016/j.jeurceramsoc.2012.10.013.

4) Ganesh I. A review on magnesium aluminate ($MgAl_2O_4$) spinel: synthesis, processing and applications). 2013. https://doi.org/10.1179/1743280412Y.0000000001.

5) Guo J, Lou H, Zhao H, Chai D, Zheng X. Dry reforming of methane over nickel catalysts supported on magnesium aluminate spinels. *Appl Catal A Gen*. 2004;273(1–2):75–82. https://doi.org/10.1016/j.apcata.2004.06.014.

6) Devanathan R, Yu N, Sickafus KE, Nastasi M, Grimsditch M, Okamoto PR. Elastic instability in ion-beam-irradiated magnesium aluminate spinel. *Philos Mag B Phys Condens Matter; Stat Mech Electron Opt Magn Prop*. 1997;75(6):793–801. https://doi.org/10.1080/13642819708205707.

7) Obradovic N, Fahrenholtz W, Filipovic S, *et al.* Characterization of MgAl2O4 sintered ceramics. *Sci Sinter*. 2019;51(4):363–376. https://doi.org/10.2298/SOS1904363O.

8) Obradović N, Fahrenholtz WG, Filipović S, *et al.* The effect of mechanical activation on synthesis and properties of $MgAl_2O_4$ ceramics. *Ceram Int*. 2019;45(9):12015–12021. https://doi.org/10.1016/j.ceramint.2019.03.095.

9) Reimanis I, Kleebe HJ. A review on the sintering and microstructure development of transparent spinel ($MgAl_2O_4$). *J Am Ceram Soc*. 2009;92(7):1472–1480. https://doi.org/10.1111/j.1551-2916.2009.03108.

10) Sokol M, Halabi M, Kalabukhov S, Frage N. Nano-structured $MgAl_2O_4$ spinel consolidated by high pressure spark plasma sintering (HPSPS). *J Eur Ceram Soc*. 2017;37:755–762. https://doi.org/10.1016/j.jeurceramsoc.2016.09.037.

11) Ye G, Troczynski T. Mechanical activation of heterogeneous sol-gel precursors for synthesis of $MgAl_2O_4$ spinel. *J Am Ceram Soc*. 2005;88(10):2970–2974. https://doi.org/10.1111/j.1551-2916.2005.00533.

12) Dwibedi D, Avdeev M, Barpanda P. Role of Fuel on Cation Disorder in Magnesium Aluminate ($MgAl_2O_4$) Spinel Prepared by Combustion Synthesis. *J Am Ceram Soc*. 2015;98(9):2908–2913. https://doi.org/10.1111/jace.13705.

13) R. J . Bratton. Co-precipitates yielding $MgAl_2O_4$ spinel powders. *American Ceramic Society Bulletin,* 48(8):759-762, 1969.

14) Li JG, Ikegami T, Lee JH, Mori T, Yajima Y. A wet-chemical process yielding reactive magnesium aluminate spinel ($MgAl_2O_4$) powder. *Ceram Int*. 2001;27(4):481–489. https://doi.org/10.1016/S0272-8842(00)00107-3.

15) Tsai MH, Yeh JW. High-entropy alloys: A critical review. *Mater Res Lett*. 2014;2(3):107–123. https://doi.org/10.1080/21663831.2014.912690.

16) Zhou J, Zhang J, Zhang F, Niu B, Lei L, Wang W. High-entropy carbide: A novel class of multicomponent ceramics. *Ceram Int*. 2018;44(17):22014–22018. https://doi.org/10.1016/j.ceramint.2018.08.100.

17) Gild J, Zhang Y, Harrington T, *et al.* High-Entropy Metal Diborides: A New Class of High-Entropy Materials and a New Type of Ultrahigh Temperature Ceramics. *Sci Rep*. 2016;6. https://doi.org/10.1038/srep37946.

18) Rost CM, Rak Z, Brenner DW, Maria JP. Local structure of the $Mg_xNi_xCo_xCu_xZn_xO$(x=0.2) entropy-stabilized oxide: An EXAFS study. *J Am Ceram Soc*. 2017;100(6):2732–2738. https://doi.org/10.1111/jace.14756.

19) Yeh JW, Chen SK, Lin SJ, *et al.* Nanostructured high-entropy alloys with multiple principal elements: Novel alloy design concepts and outcomes. *Adv Eng Mater*. 2004;6(5):299–303. https://doi.org/10.1002/adem.200300567.

20) Cantor B, Chang ITH, Knight P, Vincent AJB. Microstructural development in equiatomic multicomponent alloys. *Mater Sci Eng A*. 2004;375–377(1-2 SPEC. ISS.):213–218. https://doi.org/10.1016/j.msea.2003.10.257.

21) Rost CM, Sachet E, Borman T, *et al.* Entropy-stabilized oxides. *Nat Commun*. 2015;6:1–8. https://doi.org/10.1038/ncomms9485.

22) Dąbrowa J, Stygar M, Mikuła A, *et al.* Synthesis and microstructure of the $(Co,Cr,Fe,Mn,Ni)_3O_4$ high entropy oxide characterized by spinel structure. *Mater Lett*. 2018;216:32–36. https://doi.org/10.1016/j.matlet.2017.12.148.

23) Grzesik Z, Smoła G, Miszczak M, *et al.* Defect structure and transport properties of $(Co,Cr,Fe,Mn,Ni)_3O_4$ spinel-structured high entropy oxide.

24) Sickafus KE, Wills JM, Grimes NW. Structure of spinel. *J Am Ceram Soc*. 1999;82(12):3279–3292. https://doi.org/10.1111/j.1151-2916.1999.tb02241.

25) O'Quinn EC, Shamblin J, Perlov B, *et al.* Inversion in $Mg_{1-x}Ni_xAl_2O_4$ Spinel: New Insight into Local Structure. *J Am Chem Soc*. 2017;139(30):10395–10402. https://doi.org/10.1021/jacs.7b04370.

26) Haney EJ, Subhash G. Rate sensitive indentation response of a coarse-grained magnesium aluminate spinel. *J Am Ceram Soc*. 2011;94(11):3960–3966. https://doi.org/10.1111/j.1551-2916.2011.04756.

SECTION

3. CONCLUSIONS

The research presented in this thesis focused on the processing and atomic and microstructural properties of ceramics with the spinel crystal structure. More specifically, this research focused on the effects of composition, temperature, and mechanical activation on cation disorder within the spinel structure. Some of the overall conclusions that can be drawn from the research are as follows:

- Calcining at temperatures of 1200°C or higher was a reliable method to produce phase pure spinel ceramics from MgO and Al_2O_3 powders.
- $MgAl_2O_4$ powders produced via mechanical activation displayed lower degrees of cation disorder than powders produced through traditional ball milling routes.
- The lower inversion in MA powders (0.12 and lower) than XD powders (0.13+) can be attributed to the higher energy state of the MA materials before calcination, providing a larger driving force to reach equilibrium (zero inversion).
- The relationship between temperature and degree of inversion indicates competing mechanisms for determining cation site occupancy.
- Higher calcining temperatures appear to allow for an increase in atom mobility to reach lower inversion values but can also result in more thermally-activated site disorder.
- The high-entropy spinel composition of $(Co_{0.2}Cu_{0.2}Mg_{0.2}Ni_{0.2}Zn_{0.2})Al_2O_4$ along with the NAS and NMAS materials were all found to be highly inverse, whereas the MAS material was only about 10% inverted.

- Mechanical activation proved to be an effective method for eliminating large particles from the powder mixtures to increase the SSA of the powders.
- Hot-pressing was a reliable method to densify $(Co_{0.2}Cu_{0.2}Mg_{0.2}Ni_{0.2}Zn_{0.2})Al_2O_4$ ceramics.
- Vickers' hardness values of the HES materials were all around or above 14 GPa, higher than hardness values of transparent MAS at the same load.

The XD, non-mechanically activated $MgAl_2O_4$, materials showed a clear relationship with increasing temperature and decreasing cation disorder. This decrease in disorder at increasing temperatures is attributed to the higher mobility of the cations at higher temperatures, allowing for them to shift closer to their equilibrium positions. However, the MA powders did not appear to have a clear trend with temperature. The MA60-1200C material had an inversion value of about 0.12 and that value decreased for the next two samples as well. In contrast, the MA60-1500C material had an increased value (from the previous two) to approximately 0.10. The decrease in inversion with this set of materials was thought to be the same mechanism as seen in the XD materials but the material for 1500°C seems to display an effect of competing mechanisms for cation site disorder.

4. FUTURE WORK

Research presented in this thesis showed how the atomic and microstructural properties of spinel-based ceramics changed based on both the powder processing and calcination temperatures. Future work could help answer questions that still remain about the relationships between temperature/composition and cation site disorder. In addition, future work could also suggest processing methods that could be utilized by industry to produce these ceramics. The suggestions presented in this section strive to close the gap between laboratory investigations and industrial production methods.

To identify mechanisms that contribute to site occupancy, longer mechanical activation times and/or high calcining temperatures should be studied. It would also be worthwhile to investigate how the degree of inversion affects other material properties such as dielectric constant, band-gap energy and magnetic properties, etc. This would allow a further customization of materials for advanced applications.

Dense ceramic materials examined in this thesis were produced by hot-pressing. Pressureless sintering of the $(Co_{0.2}Cu_{0.2}Mg_{0.2}Ni_{0.2}Zn_{0.2})Al_2O_4$ material would make HES ceramics more attractive in an industry setting where pressureless sintering helps to lower processing costs. The densification kinetics differ between hot-pressing and pressureless sintering. Any potential changes to the microstructure through pressureless sintering could change the hardness (and other mechanical properties) exhibited by sintered $(Co_{0.2}Cu_{0.2}Mg_{0.2}Ni_{0.2}Zn_{0.2})Al_2O_4$ ceramics compared to the hot-pressed materials examined in this study.

Powder processing was carried out by dry-ball milling; however, aqueous based processing (as seen in Paper II) could reduce environmental concerns and lower costs over a dry based approach. In order to optimize an aqueous based processing method, research on the effectiveness of sintering aids would be required due to the increased hydroxylation of oxide powders during aqueous milling. The final ceramic would still be a spinel ceramic, the advantages of aqueous processing are cutting down dust in the environment, machine wear and tear, all of which would cut overall processing costs.

Along with the above-mentioned studies, determining the effects of each cation on site occupancy in the high-entropy spinel would be worthy, as composition is known to effect site disorder. Also, general property measurements such as mechanical strength and dielectric properties would contribute to the field of high entropy materials.

REFERENCES

1) Ganesh I. A review on magnesium aluminate ($MgAl_2O_4$) spinel: synthesis, processing and applications). 2013. https://doi.org/10.1179/1743280412Y.0000000001.

2) Guo J, Lou H, Zhao H, Chai D, Zheng X. Dry reforming of methane over nickel catalysts supported on magnesium aluminate spinels. *Appl Catal A Gen.* 2004;273(1–2):75–82. https://doi.org/10.1016/j.apcata.2004.06.014.

3) Devanathan R, Yu N, Sickafus KE, Nastasi M, Grimsditch M, Okamoto PR. Elastic instability in ion-beam-irradiated magnesium aluminate spinel. *Philos Mag B Phys Condens Matter; Stat Mech Electron Opt Magn Prop.* 1997;75(6):793–801. https://doi.org/10.1080/13642819708205707.

4) Ianoş R, Lazău I, Păcurariu C, Barvinschi P. Solution combustion synthesis of MgAl2O4 using fuel mixtures. *Mater Res Bull.* 2008;43(12):3408–3415. https://doi.org/10.1016/j.materresbull.2008.02.003.

5) Esposito L, Piancastelli A, Martelli S. Production and characterization of transparent $MgAl_2O_4$ prepared by hot pressing. *J Eur Ceram Soc.* 2013;33(4):737–747. https://doi.org/10.1016/j.jeurceramsoc.2012.10.013.

6) Rd B, Wooo J, Nrns Q, Rnrcx KQ, Monrnz B. Order-disorder phenomena in MgAlrO4 spinel. 1986..

7) Ball JA, Grimes RW, Price DW. Predicting lattice parameter as a function of cation disorder in $MgAl_2O_4$ spinel. 2005. https://doi.org/10.1088/0953-8984/17/48/014

8) U. Schmocker, H. R. Boesch, and F. Waldner. A Direct Determination of Cation Disorder in the $MgAl_2O4$ Spinel by ESR. *Phys. Lett.,* 40A(3):237- 38, 1972.

9) Brankovic´ A. Mechanochemical activation of (SeO2 ? Na2CO3) mixture and sodium selenite synthesis in vibrational mill. J Sol State Chem. 1998;135:256–9.

10) Obradovic´ N, Filipovic´ S, Pavlovic´ V, Mitric´ M, Markovic´ S, Mitic´ V, Đordevic N, Ristic MM. Isothermal sintering of barium– zinc–titanate ceramics. Ceram Int. 2011;37:21–7.

11) Kostic´ E. Activation of solid-state processes in sintering and materials. Beijing: International Academic Publishers; 1995. p. 142–7.

12) Pavlovic´ M, Andric´ LJ, Radulovic´ D, Drmanic´ S, Đordevic N, Petrov M. Influence of mechanical activation of a cordierite- based filler on sedimentation stability of lost foam refractory coatings. Sci Sinter. 2019; 51:15–25.

13) W. H. Bragg. The Structure of the Spinel Group Crystals. *Philos. Mag.,* 30 :305-315, 1915.

14) S. Nishikawa. Structure of Some Crystals of Spinel Group. *Proc. Phys. Soc. Tokyo* , 8:199-209, September 1915.

15) Royal Society of London. Series A, Mathematical and Physical Science. *New Symmetry and Structure for Spinel,* volume 386. The Royal Society, April 1983.

16) Sickafus KE, Wills JM, Grimes NW. Structure of Spinel. *J Am Ceram Soc*. 2004;82(12):3279–3292. https://doi.org/10.1111/j.1151-2916.1999.tb02241.

17) Shukla P, Chernatynskiy A, Nino JC, Sinnott SB, Phillpot SR. Effect of inversion on thermoelastic and thermal transport properties of MgAl2O4 spinel by atomistic simulation. *J Mater Sci*. 2011;46(1):55–62. https://doi.org/10.1007/s10853-010-4795-7.

18) T . F. W. Barth and E. Posnjak. Crystallography - the spinel structure: An example of variae atom equipoints. *Journal of the Washington Academy of Sciences,* 21(12):255- 258, June 1931.

19) Posnjak E, Barth TFW. A new type of crystal fine-structure: Lithium ferrite (Li2O·Fe2O3). *Phys Rev*. 1931;38(12):2234–2239. https://doi.org/10.1103/PhysRev.38.2234.

20) T. F. W. Barth and E. Posnjak. Spinel structure: With and without variate atom equipoints. *Z. Kristallogr.,* 82:325- 341, 1932.

21) Verwey EJW, Heilmann EL. Physical properties and cation arrangement of oxides with spinel structures I. Cation arrangement in spinels. *J Chem Phys.* 1947;15(4):174–180. https://doi.org/10.1063/1.1746464.

22) Sickafus KE, Wills JM, Chen SP, Terry Jr JH, Hartmann T, Sheldon RI. Development of a Fundamental Understanding of Chemical Bonding and Electronic Structure in Spinel Compounds. Technical Report 96257, Los Alamos National Labs, 1999. 1-61 pp.

23) Wood BJ, Kirkpatrick RJ, Montez B. Order-disorder phenomena in $MgAl_2O_4$ spinel. *Am Mineral.* 1986;71(7–8):999–1006.

24) Sickafus KE, Wills JM, Chen SP, Terry Jr JH, Hartmann T, Sheldon RI. Development of a Fundamental Understanding of Chemical Bonding and Electronic Structure in Spinel Compounds. 1999.

25) W. D. Kingery, Chiang Y-M, III. DPB. Physical Ceramics: Principles for Ceramic Science and Engineering. John Wiley & Sons, Inc.; 1997.

26) Park HC, Lee YB, Oh KD, Riley FL. Grain growth in sintered $MgAl_2O_4$ spinel. *J Mater Sci Lett.* 1997;16(22):1841–1844. https://doi.org/10.1023/A:1018585105949.

27) C. R. Bickmore, K F . Waldner, D. R. Treadwell, and R. M. Laine. Ultrafine Spinel Powders by Flame Spray Pyrolysis of a Magnesium Aluminum Alkoxide. *J. Am. Ceram. Soc.,* 79(5):1419-1423, 1996.

28) R. J . Bratton. Co-precipitates yielding $MgAl_2O_4$ spinel powders. *American Ceramic Society Bulletin,* 48(8):759-762, 1969.

29) M. Barj, J. F. Bocquet, K. Chhor, and C. Pommier. Submicronic $MgA1_2O_4$ powder synthesis in supercritical ethanol. *J. Mater. Sci.,* 27(8):2187, 1992.

30) N. Yang and L. Chang. Structural inhomogeneity and crystallization behavior of aerosol-reacted $MgAl_2O_4$ powders. *Mater. Let.* , 15(1-2):84-88, 1992.

31) O. Varnier, N. Hovnanian, A. Larbot, P. Bergez, L. Cot, and J . Charpin. Sol-gel synthesis of magnesium aluminum spinel from a heterometallic alkoxide. *Mater. Res. Bull.,* 29(5):479- 488, 1994.

32) Li JG, Ikegami T, Lee JH, Mori T, Yajima Y. A wet-chemical process yielding reactive magnesium aluminate spinel (MgAl2O4) powder. *Ceram Int.* 2001;27(4):481–489. https://doi.org/10.1016/S0272-8842(00)00107-3.

33) Tripathi HS, Mukherjee B, Das S, Haldar MK, Das SK, Ghosh A. Synthesis and densification of magnesium aluminate spinel: Effect of MgO reactivity. *Ceram Int.* 2003;29(8):915–918. https://doi.org/10.1016/S0272-8842(03)00036-1.

34) Bratton RJ. Initial Sintering Kinetics of $MgAl_2O_4$. *J Am Ceram Soc.* 1969;52(8):417–419. https://doi.org/10.1111/j.1151-2916.1969.tb11971.

35) Bratton RJ, Terwilliger GR, Ho SM. Densification phenomena in the hot-pressing of spinel. *J Mater Sci.* 1972;7(12):1363–1368. https://doi.org/10.1007/BF00574926.

36) Rahaman MN. Ceramic Processing. Second Edition. Taylor & Francis Group, LLC; 2017.

37) Sokol M, Ratzker B, Kalabukhov S, Dariel MP, Galun E, Frage N. Transparent Polycrystalline Magnesium Aluminate Spinel Fabricated by Spark Plasma Sintering. *Adv Mater.* 2018;30(41):1–11. https://doi.org/10.1002/adma.201706283.

38) Rubat Du Merac M, Reimanis IE, Kleebe HJ. Electrochemical Impedance Spectroscopy of Transparent Polycrystalline Magnesium Aluminate (MgAl2O4) Spinel. *J Am Ceram Soc.* 2015;98(7):2130–2138. https://doi.org/10.1111/jace.13596.

39) Morita K, Kim BN, Hiraga K, Yoshida H. Fabrication of transparent MgAl2O4 spinel polycrystal by spark plasma sintering processing. *Scr Mater*. 2008;58(12):1114–1117. https://doi.org/10.1016/j.scriptamat.2008.02.008.

40) K.J.D. Mackenzie, J. Temuujin, T.S. Jadambaa, M.E. Smith, P. Angerer, J. Mater. Sci. 35 (2000) 5529–5535.

41) Rahaman MN. Ceramic processing and sintering, second edition. 2017 https://doi.org/10.1201/9781315274126.

42) Tavangarian F, Emadi R. Synthesis and characterization of pure nanocrystalline magnesium aluminate spinel powder. *J Alloys Compd*. 2010;489(2):600–604. https://doi.org/10.1016/j.jallcom.2009.09.120.

43) Sheldon RI, Hartmann T, Sickafus KE, *et al.* Cation Disorder and Vacancy Distribution in Nonstoichiometric Magnesium Aluminate Spinel, MgO·xAl2O3. *J Am Ceram Soc*. 2004;82(12):3293–3298. https://doi.org/10.1111/j.1151-2916.1999.tb02242.

44) O'Quinn EC, Shamblin J, Perlov B, *et al.* Inversion in Mg1-xNixAl2O4 Spinel: New Insight into Local Structure. *J Am Chem Soc*. 2017;139(30):10395–10402. https://doi.org/10.1021/jacs.7b04370.

45) Pellerin N, Dodane-Thiriet C, Montouillout V, Beauvy M, Massiot D. Cation sublattice disorder induced by swift heavy ions in MgAl 2O4 and ZnAl2O4 spinels: 27Al solid-state NMR study. *J Phys Chem B*. 2007;111(44):12707–12714. https://doi.org/10.1021/jp072620t.

46) Peterson RC, Lager GA, Hitterman EL. A time-of-flight neutron powder diffraction study of MgAl2O 4 at tempratures up to 1273 K. *Am Mineral*. 1991;76(9–10):1455–1458.

47) Redfern SAT, Harrison RJ, O'Neill HSC, Wood DRR. Thermodynamics and kinetics of cation ordering in MgAl2O4 spinel up to 1600 °C from in situ neutron diffraction. *Am Mineral*. 1999;84(3):299–310. https://doi.org/10.2138/am-1999-0313

48) Ball JA, Pirzada M, Grimes RW, Zacate MO, Price DW, Uberuaga BP. Predicting lattice parameter as a function of cation disorder in MgAl 2O4 spinel. *J Phys Condens Matter*. 2005;17(48):7621–7631. https://doi.org/10.1088/0953-8984/17/48/014.

49) Obradović N, Fahrenholtz WG, Filipović S, *et al.* Formation kinetics and cation inversion in mechanically activated MgAl 2 O 4 spinel ceramics. *J Therm Anal Calorim*. 2020;140(1):95–107. https://doi.org/10.1007/s10973-019-08846-w.

50) Obradović N, Fahrenholtz WG, Filipović S, *et al.* Formation kinetics and cation inversion in mechanically activated $MgAl_2O_4$ spinel ceramics. *J Therm Anal Calorim*. 2020;140(1):95–107. https://doi.org/10.1007/s10973-019-08846-w.

51) Tsai MH, Yeh JW. High-entropy alloys: A critical review. *Mater Res Lett*. 2014;2(3):107–123. https://doi.org/10.1080/21663831.2014.912690.

52) Zhou J, Zhang J, Zhang F, Niu B, Lei L, Wang W. High-entropy carbide: A novel class of multicomponent ceramics. *Ceram Int*. 2018;44(17):22014–22018. https://doi.org/10.1016/j.ceramint.2018.08.100.

53) Gild J, Zhang Y, Harrington T, *et al.* High-Entropy Metal Diborides: A New Class of High-Entropy Materials and a New Type of Ultrahigh Temperature Ceramics. *Sci Rep*. 2016;6. https://doi.org/10.1038/srep37946.

54) Rost CM, Rak Z, Brenner DW, Maria JP. Local structure of the $Mg_xNi_xCo_xCu_xZn_xO(x=0.2)$ entropy-stabilized oxide: An EXAFS study. *J Am Ceram Soc*. 2017;100(6):2732–2738. https://doi.org/10.1111/jace.14756.

55) Yeh JW, Chen SK, Lin SJ, *et al.* Nanostructured high-entropy alloys with multiple principal elements: Novel alloy design concepts and outcomes. *Adv Eng Mater*. 2004;6(5):299–303. https://doi.org/10.1002/adem.200300567.

56) Cantor B, Chang ITH, Knight P, Vincent AJB. Microstructural development in equiatomic multicomponent alloys. *Mater Sci Eng A*. 2004;375–377(1-2 SPEC. ISS.):213–218. https://doi.org/10.1016/j.msea.2003.10.257.

57) Rost CM, Sachet E, Borman T, *et al.* Entropy-stabilized oxides. *Nat Commun*. 2015;6:1–8. https://doi.org/10.1038/ncomms9485.

58) Gurao NP, Biswas K. High-entropy materials: Critical review and way forward. *Curr Sci*. 2020;118(10):1520–1539. https://doi.org/10.18520/cs/v118/i10/1520-1539.

59) Mao A, Xiang HZ, Zhang ZG, Kuramoto K, Yu H, Ran S. Solution combustion synthesis and magnetic property of rock-salt (Co 0.2 Cu 0.2 Mg 0.2 Ni 0.2 Zn 0.2)O high-entropy oxide nanocrystalline powder. *J Magn Mater*. 2019;484:245–252. https://doi.org/10.1016/j.jmmm.2019.04.023.

60) Zhang RZ, Reece MJ. Review of high entropy ceramics: design, synthesis, structure and properties. *J Mater Chem A*. 2019;7(39):22148–22162. https://doi.org/10.1039/c9ta05698j.

61) Dąbrowa J, Stygar M, Mikuła A, *et al.* Synthesis and microstructure of the (Co,Cr,Fe,Mn,Ni)3O4 high entropy oxide characterized by spinel structure. *Mater Lett*. 2018;216:32–36. https://doi.org/10.1016/j.matlet.2017.12.148.

62) Grzesik Z, Smoła G, Miszczak M, *et al.* Defect structure and transport properties of $(Co,Cr,Fe,Mn,Ni)_3O_4$ spinel-structured high entropy oxide.

VITA

Cole Corlett was born on August 28th, 1994 in Joplin, Missouri. He would live in Joplin until moving to Webb City, Missouri in 2011 where he would eventually graduate from in the spring of 2013. Cole enrolled in classes at Missouri Southern State University in Joplin for the upcoming fall semester. By the spring semester of his sophomore year, he had declared a double major of Chemistry and Biochemistry. During his four and half years at MSSU, Cole was a member of the MSSU Chemistry Club and Omicron Delta Kappa. In the spring of his junior year, Cole was elected to President of the Chemistry Club. As part of his undergraduate research, Cole attended Missouri Academy of Science in the spring of 2017 to represent the Chemistry department along with good friends and mentors. During his undergraduate career, Cole work for Jayhawk Fine Chemicals as an chemist intern in the Research & Development lab. It was this experience that made him decide to attend graduate school. Cole received his B.S. degree in Chemistry & Biochemistry from Missouri Southern State University in December of 2017.

Cole began his graduate work for Dr. William Fahrenholtz at the Missouri University of Science and Technology in May of 2018. During his graduate career, Cole focused his research on the processing and properties of magnesium-aluminate spinel-based ceramics. He also assisted with the ceramics processing lab, published two papers and helped with demonstrations during summer camps. Cole received his M.S. degree in Materials Science and Engineering from Missouri University of Science and Technology in May of 2021.